Correspondence to:
D. M. Gaiero,
dgaiero@efn.uncor.edu

Soluble iron inputs to the Southern Ocean through recent andesitic to rhyolitic volcanic ash eruptions from the Patagonian Andes

L. E. Simonella[1], M. E. Palomeque[1], P. L. Croot[2], A. Stein[3], M. Kupczewski[4], A. Rosales[4], M. L. Montes[5], F. Colombo[1], M. G. García[1], G. Villarosa[6], and D. M. Gaiero[1]

[1]Centro de Investigaciones en Ciencias de la Tierra (CONICET)-FCEFyN-Universidad Nacional de Córdoba, Córdoba, Argentina, [2]Earth and Ocean Sciences, School of Natural Sciences, National University of Ireland Galway, Galway, Ireland, [3]ERT, Inc., College Park, Maryland, USA, [4]Departamento de Física, Facultad de Ingeniería, Universidad Nacional de la Patagonia San Juan Bosco, Trelew, Argentina, [5]Departamento de Física, Facultad de Ciencias Exactas, Universidad Nacional de La Plata, Instituto de Física La Plata-CONICET, La Plata, Argentina, [6]INIBIOMA, CONICET, Universidad Nacional del Comahue, Bariloche, Argentina

Abstract Patagonia, due to its geographic position and the dominance of westerly winds, is a key area that contributes to the supply of nutrients to the Southern Ocean, both through mineral dust and through the periodic deposits of volcanic ash. Here we evaluate the characteristics of Fe dissolved (into soluble and colloidal species) from volcanic ash for three recent southern Andes volcanic eruptions having contrasting features and chemical compositions. Contact between cloud waters (wet deposition) and end-members of andesitic (Hudson volcano) and rhyolitic (Chaitén volcano) materials was simulated. Results indicate higher Fe release and faster liberation rates in the andesitic material. Fe release during particle-seawater interaction (dry deposition) has higher rates in rhyolitic-type ashes. Rhyolitic ashes under acidic conditions release Fe in higher amounts and at a slower rate, while in those samples containing mostly glass shards, Fe release was lower and faster. The 2011 Puyehue eruption was observed by a dust monitoring station. Puyehue-type eruptions can contribute soluble Fe to the ocean via dry or wet deposition, nearly reaching the limit required for phytoplankton growth. In contrast, the input of Fe after processing by an acidic eruption plume could raise the amount of dissolved Fe in surface ocean waters several times, above the threshold required to initiate phytoplankton blooms. A single eruption like the Puyehue one represents more than half of the yearly Fe flux contributed by dust.

1. Introduction

Iron is considered a limiting nutrient for phytoplankton growth in extensive areas of the ocean [e.g., *Martin et al.*, 1990; *Jickells et al.*, 2005]. Fe is a required element for phytoplankton as it has a key role in several important metabolic pathways, such as photosynthesis, nitrate assimilation, and nitrogen fixation [e.g., *Sunda and Huntsman*, 1995; *Falkowski et al.*, 1998; *Morel and Price*, 2003]. Atmospheric continental particles, primarily originating from desert regions, constitute an important source of Fe to surface seawater. The atmosphere is the exclusive transport agent from deserts to remote areas of the ocean. In some of these remote oceanic areas, Fe is thought to limit the biomass of phytoplankton population; these areas are referred to as high-nutrient low-chlorophyll (HNLC) regions. One important HNLC region is the Southern Ocean, which represents about 20% of the total global ocean and plays a major role in the distribution of carbon dioxide between atmospheric and oceanic reservoirs [e.g., *Jickells et al.*, 2005]. This oceanic region is atypical, as it exhibits plenty of major plant nutrients on surface water, but somehow, the photosynthetic CO_2 fixation and plant biomass is low.

Dust supply to the Southern Ocean increased during glacial periods; evidence indicates a firm connection between dust input and the appearance of the deep glaciations, characterizing the last past million years of Earth's history [*Martínez-Garcia et al.*, 2011]. Evidences indicate that ocean surface Fe fertilization through major volcanic eruptions could have had important consequences on atmospheric CO_2 levels during the Earth's past [e.g., *Sarmiento et al.*, 1993; *Watson*, 1997; *Cather et al.*, 2009; *Langmann et al.*, 2010]. In the Southern Ocean, paleorecord archives from drill cores show enhanced diatom growth following volcanic ash deposition ~450 ka ago, which suggests a possible fertilization of these oceanic waters [*Kunz-Pirrung et al.*, 2002]. Assisted by new technology (i.e., satellite imagery and transport particle models) improved

observation of seasonal and spatial evolution of worldwide volcanic eruptions and the environmental impact of volcanic ash in water on the ocean's surface is now possible. For example, it is believed that the ash input onto surface ocean waters following the 1991 Pinatubo eruption resulted in massive plankton growth, thus promoting transient enhanced fixation of atmospheric CO_2 [*Sarmiento*, 1993]. Although the impact on atmospheric CO_2 was not significant, the 2008 Kasatochi eruption provided evidence that volcanic ash stimulates blooms in the subarctic NE Pacific [*Hamme et al.*, 2010]. Recent results from bottle enrichment experiments in the NE Pacific and Southern Ocean have demonstrated a positive phytoplankton community response to the addition of volcanic ash [*Mélançon et al.*, 2014; *Browning et al.*, 2014]. In general, these observations indicate that the fertilizing potential of volcanic ashes on the marine environment is not yet well understood.

For phytoplankton to utilize the Fe present in airborne materials, some fraction of this micronutrient must be first mobilized into an available form in oceanic waters. Recent efforts have been dedicated to investigating Fe bioavailability present in dust sourced in arid continental areas and its effects on fertilizing the ocean [e.g., *Shi et al.*, 2012, and citations therein]. However, only a small number of studies have documented different aspects related to the release of Fe from volcanic ash into freshwater and seawater [*Duggen et al.*, 2007; *Frogner et al.*, 2001; *Jones and Gislason*, 2008; *Olgun et al.*, 2011, 2013; *Ruggieri et al.*, 2012; *Durant et al.*, 2012; *Achterberg et al.*, 2013; *Olsson et al.*, 2013].

Due to its geographic position and the dominance of westerly winds, Patagonia is viewed as a key area for supplying Fe through mineral dust [e.g., *Gaiero et al.*, 2003; *Gassó and Stein*, 2007; *Gassó et al.*, 2010]. In recent decades, the occurrence of important volcanic eruptions in the Patagonian Andes has also highlighted the significance of episodic inputs of volcanic ash to the Southern Ocean. However, ash fall, fluxes, and characteristics of Fe inputs onto the ocean surface have never been studied in depth. Therefore, the amount of Fe released by volcanic ash is a major source of uncertainty in modeling Fe deposition and dissolution onto the ocean surface.

The aim of this contribution is to evaluate the characteristics of the soluble Fe pool present in pristine volcanic ash from three recent Andean volcanic eruptions of differing eruptive features and diverse chemical compositions (i.e., volcanic eruptions from Hudson 1991, Chaitén 2008, and Puyehue 2011). The mobilization of Fe from ashes into soluble forms is investigated via two mechanisms: "dry deposition" through direct mobilization from dry ash upon contact with seawater and "wet deposition," where Fe mobilizes from ash during interaction with plume/cloud water and plume/acidified cloud water before entering into contact with surface seawater. These results are contrasted with similar experiments run on Patagonian dust and topsoil samples. We also discussed the fluxes of soluble Fe into the ocean and their possible effects on the marine primary production.

2. Volcanic Events Main Features

The Hudson eruptions took place on 8–9 and 12–15 August 1991. These eruptions produced ~4.3 km^3 ash bulk volume on land, while an estimated ~1.1 km^3 was deposited onto the iron-limited Atlantic sector of the Southern Ocean. Density of this material was ~ 2.5 g cm^{-3} and would represent >2000 Tg deposited over the ocean during 5 days which is about the same as the total amount of dust deposited on the continents and oceans in 1 year [*Mahowald et al.*, 2006]. The composition of the tephra ranged from basaltic to trachyandestic [*Scasso et al.*, 1994]. This event is considered to be one of the largest historical eruptions in South America [*Kratzmann et al.*, 2009]. On 15 August, tephra from the last phase of the eruption was transported ~1500 km to the SE, which had a direct impact on the city of San Julián (49°05′S/67°43′W). Two weeks after the main eruption, several centimeters of ash accumulation were observed on the grounds of the Malvinas Island (>2700 km from Cerro Hudson) [*Smellie*, 1999]. Similarly, 2 months after the eruption had ended, satellite observations indicated that westerly winds had remobilized and transported ashes from the vicinity of the volcano >1000 km to the southern Atlantic Ocean [*Global Volcanism Network Bulletin*, 1991]. Deposits in the vicinity of this volcano reveal at least 12 explosive eruptions from the Holocene to Recent [*Naranjo and Stern*, 1998].

On 2 May 2008, the Chaitén volcano unexpectedly erupted, producing an ash column exceeding 21 km above sea level [*Lara*, 2009]. Compared to the Hudson, the Chaitén eruption showed a rhyolitic composition, which, in a regional context, is unusual for the southern volcanic zone (SVZ) of the southern Andes. At the

Table 1. Summary of Patagonian Ash Samples Collected in This Study

Volcano	Sampling Locality	Sample ID	Collection Date	Geographic Position	Distance (km)	Comments
Puyehue	Bariloche	P1	4 June 2011	41°09′S/71°18′W	110	direct fallout sampled/plastic bags
Puyehue	Bariloche	P2	17 June 2011	41°09′S/71°18′W	110	direct fallout sampled/plastic bags
Puyehue	Comallo	P3	13 June 2011	41°01′S/70°16′W	200	direct fallout sampled/plastic bags
Puyehue	Cutral-Có	P4	10–12 June 2014	38°55′S/69°14′W	350	balcony of house
Puyehue	Gral. Roca	P5	12 June 2014	39°01′S/67°34′W	450	window of house
Puyehue	Trelew	P6	3–6 June 2011	43°14′S/65°19′W	600	direct fallout sampled/dust trap
Puyehue	Trelew	P7	6–9 June 2011	43°14′S/65°19′W	600	direct fallout sampled/dust trap
Puyehue	Trelew	P8	9–14 June 2011	43°14′S/65°19′W	600	direct fallout sampled/dust trap
Hudson	San Julian	HUD	12–15 August 2001	49°05′S/67°43′W	550	roof of house
Chaitén	El Bolsón	CH1	6 May 2008	41°58′S/71°30′W	110	ground
Chaitén	Epuyen	CH2	9 May 2008	42°53′S/71°21′W	140	ground

global level, there are few historical examples of rhyolitic eruptions such as Chaitén [*Watt et al.*, 2009]. Compared to the 1991 Hudson eruption, Chaitén contributed a modest total ash deposit volume, estimated to be 0.5–1.0 km^3 [*Alfano et al.*, 2011]. The ash plume reached the ocean, as indicated by satellite Atmospheric Infrared Sounder imagery near South Africa [*Gangale et al.*, 2010], Moderate Resolution Imaging Spectroradiometer (MODIS) images, and model simulations [*Folch et al.*, 2008]. It was estimated that about 5% (i.e., ~9×10^9 kg or 8×10^{-3} km^3), mostly <50 μm grain size, fell over the Atlantic Ocean [*Watt et al.*, 2009]. A previous documented eruption of this volcano occurred about 10 kyr ago [*Naranjo and Stern*, 2004]. However, a recent study based on tephrochronological data from lake records in Argentina indicates other important explosive events during the Holocene [*Iglesias et al.*, 2012].

On 4 June 2011 the Puyehue-Cordón Caulle volcano complex erupted (from now we refer to this event as Puyehue), injecting large amounts of volcanic ash into the atmosphere (column over 12 km high) and depositing a thick blanket of pumice on the surrounding landscape. According to observations, the initial phase of the eruption lasted 16 days (1–20 June) [*Collini et al.*, 2013]. The ash plume circumnavigated the Earth and persisted for weeks. On 14 June, parts of the emitted ash returned to the source region from the west. This suggests that a significant mass of the original erupted material was deposited over the ocean (see section 4.3). This volcanic complex preserved ~131 km^3 of lava and tephra that erupted from numerous episodes that were widely separated in time and space. For the last eruption, ash accumulation of 0.2 to 10 mm thickness was observed ~1200 km along the Patagonian coast [*Bermudez and Delpino*, 2011] with an estimated deposition of ~ 100 g m^{-2} [*Collini et al.*, 2013]. The modern Puyehue stratovolcano was built during the past 69 kyr, following a hiatus of 25 kyr. Puyehue erupted ~15 km^3 of basaltic to rhyolitic magma that spans the entire compositional range found in the SVZ [*Singer et al.*, 2008].

3. Material and Methods

3.1. Sampling

Some features of the ash samples used in this study are summarized in Table 1. Samples Hud and P1–P5 were collected by local inhabitants, known to us, who had previously been instructed on how to collect samples of pure ash. Basically, the material was collected in open plastic bags before reaching the ground (i.e., P1–P3) or they were taken after the ash had been deposited on the roof, balcony, or windows of houses (i.e., Hud, P4, and P5). Samples Ch1 and Ch2 were collected by one of us (G.V.) using a plastic shovel to take the first centimeter of the deposited ash and avoiding contact with existing soil material.

A dust monitoring station located in Trelew (43°14′S/65°19′W) near the Patagonian coast permitted the direct fallout sampling of volcanic ashes from the Puyehue eruptions (samples P6–P8). This monitoring site is equipped with a pyramidal receptacle (CP) that is suited to measure vertical fluxes [*Orange et al.*, 1990; *Gaiero et al.*, 2003, 2013; *Goossens and Rajot*, 2008; *Skonieczny et al.*, 2011]. Along with this, an isokinetic BSNE (Bufalo Spring Number Eigth) [*Fryrear*, 1986] trap was used to estimate horizontal dust fluxes and dust concentrations [e.g., *Goossens and Buck*, 2012]. Both traps were placed on the roof (height ~15 m) of a building on the Trelew University campus in order to avoid collecting local saltation material. Compared to similar collectors designed to estimate dust deposition, the efficiency of the CP trap is only 30% [*Goossens and Rajot*, 2008]. The Trelew station ran automatically for about 14 days, after which an operator collected

Table 2. Iron Dissolution Experiments Performed on Patagonian Ash, Topsoil, and Dust Samples by Means of Two Different Methods: CF (Continuous Flow Method) and Batch Using Seawater (SW)[a]

Sample ID	Al$_2$O$_3$ <63μm	Al$_2$O$_3$ <11μm	SiO$_2$ <63μm	SiO$_2$ <11μm	Fe$_2$O$_3$ <63μm	Fe$_2$O$_3$ <11μm	TiO$_2$ <63μm	TiO$_2$ <11μm	Fe^{2+} <63μm %	Fe^{+3} %	Conductivity <63μm μS/cm	pH <63μm	Fe$_{DI}$ <63μm	Fe$_{WA}$ <63μm	Fe$_{DI}$ <11μm	Fe$_{WA}$ <11μm	Fe$_{SW}$ <63μm	Mode (μm) <63μm
	wt %								%	%			μg g^{-1}					
P1[b]	12.8	13.8	68.0	68.1	4.9	4.5	0.67	0.59	73	27	8.7	6.44	36±10	705±81	71±0	1460±85	20	14.1
P2[b]	13.3	13.8	68.6	68.6	4.4	4.3	0.60	0.58	74	26	13	6.90	66±4	566±125	na	na	na	16.2
P3[b]	12.8	12.7	68.6	68.9	4.5	4.5	0.61	0.61	na	na	6.9	5.84	23±5	95±37	na	na	na	42.0
P4[b]	13.2	12.7	67.3	67.9	4.7	4.6	0.64	0.62	72	28	37	7.14	27±5	396±67	na	na	na	48.1
P5[b]	13.5	12.7	66.0	66.5	4.3	4.9	0.59	0.68	63	37	87	7.19	25±12	606±131	na	na	na	48.0
P6	14.2	13.0	67.4	67.4	4.4	5.0	0.61	na	70	30	15	6.84	4±0	818±232	87±27	1595±511	6.2	14.2
P7	13.6	13.0	68.7	68.6	4.1	4.7	0.57	na	74	26	8.7	6.36	24±2	331±100	15±7	1411±185	18	21.1
P8	13.4	na	63.3	na	4.3	na	0.59	na	na	na	na	na	na	na	na	na	8.1	28.0
HUD	16.6	15.6	60.9	59.3	6.2	6.3	1.27	1.22	80	20	20	6.68	93±84	484±40	23±2	990±282	3.6	47.7
CH1[b]	13.9	14.0	72.5	71.3	1.8	2.0	0.18	0.20	71	29	13	6.76	19±13	1008±190	27±5	2172±563	32	14.2
CH2	13.8	9.9	73.4	51.0	1.7	1.4	0.16	0.13	74	26	8.0	6.24	22±12	924±95	35±3	1028±264	na	13.6
TS1	8.8	6.3	39.2	29.6	4.0	3.1	0.58	0.46	na	na	na	na	40±17	1374±166	22±2	1935±217	na	44.1
TS2[b]	13.9	12.9	53.4	49.2	4.0	6.2	0.74	0.67	18	82	na	na	37±22	1140±254	17±10	1077±141	na	7.2
Tw-dust[c]	16.7	na	64.1	na	5.8	na	0.91	na	na	na	na	na	12±6	2684±686	na	na	3.9	13.5

[a]Also shown are other relevant information for the discussion of the data (see section 3). DI, deionized water; WA, weak acid (1% HNO$_3$); na, not available.
[b]Fe Solubility data taken from Simonella et al. [2014].
[c]Bulk sample.

the samples using a vacuum pump to filter (through dry or wet medium) and retain particles on a pre-weighed 0.45 μm membrane. At the same time, the operator retrieved the recorded data from the weather station located on the same pole as the dust catchers. Fifteen 30 min average wind speeds were measured at a height of 15 m, next to the BSNE collectors.

All these samples were collected dry a few hours after the different volcanic eruption phases. The samples were stored using polyethylene bags and then, for long-term storage, they were dried in an oven at 40°C and stored in airtight plastic bottles until analyses.

Dust storm samples usually represent the average composition of sediments from different, remote source areas and ultimately can better represent the atmospheric input into the ocean [e.g., Gaiero et al., 2013]. For this study, we also included soluble Fe data from dust samples collected during three different dust storms that impacted the Trelew station, as well as data from two topsoil samples (TS, upper 5 cm) collected from nearby ephemeral lakes singled out as important Patagonian dust emission areas [e.g., Johnson et al., 2010] (Table 2). The scarce mass of sediment obtained in each of these dust events allows for only a partial characterization of the different variables considered in this contribution. We then adopted a generic name, Tw-dust, to refer to data obtained from the composite dust samples collected at this site.

3.2. Characterization of Ash Samples
3.2.1. Grain Size Analyses
The fractionation of mineral dust according to grain size could exert an important control on Fe solubility [e.g., Ayris and Delmelle, 2012, and citations therein]. One critical aspect of evaluating Fe solubility from ash

particles is the particle size distribution of the samples. During long-range transport, atmospheric dust particles of up to 70 μm can be carried long distances from the source (>2000 km) [*Gaiero et al.*, 2013]. In order to homogenize the ground samples for Fe availability studies and mimic the dominant grain size distribution obtained in samples collected at the monitoring site, they were dry sieved using <63 μm plastic mesh. During atmospheric transport, particles tend to be finer with increasing distance from the emission center, as they have a longer residence time in the atmosphere and a higher possibility of being deposited over distant oceanic areas. In general, model estimations and data from research cruises measuring nutrient inputs into the ocean provide estimates of particles with a diameter of <11 μm [e.g., *Li et al.*, 2008; *Johnson et al.*, 2010; *Baker et al.*, 2013]. Due to time constraints and the scarcity of material, only a few ash samples and the ashes collected at the monitoring site were dry sieved using a <11 μm plastic mesh.

Grain size distribution of the volcanic ashes was measured by laser diffraction, using a Horiba LA 950 particle size analyzer. Samples were not dispersed to prevent the breaking up of aggregates. The precision (reproducibility) of the laser diffraction particle sizer was tested by using mixtures of glass beads (National Institute of Standards and Technology (NIST) traceable polydisperse particle standard PS202/3–30 μm and PS215/10–100 μm, Whitehouse Scientific). For both runs (PS202, $n = 6$ and PS215, $n = 5$), the median (D50) was within 3% of the certified nominal value, and the percentiles D10 and D90 were within 5% of nominal values for the standards. Most of the samples show bimodal grain size distributions. Table 2 shows the main grain size mode values obtained for ash, topsoils, and dust samples.

3.2.2. Characterization and Quantification of Glass Shard and Crystalline Minerals in Volcanic Ashes
Modal percentages of transparent (isotropic and anisotropic) and opaque phases were determined by point counting of loose grains (fraction <63 μm) under a polarizing microscope. For each sample, a total of 1000 loose grains were counted. The crystalline phases were characterized by X-ray diffraction (XRD) analysis using a PANanalytical X'pert PRO instrument (Cu$K\alpha$, radiation, obtained at 40 kV and 40 mA). XRD data were obtained for random samples in the 2θ range from 5 to 60° (step size: 0.02; 13 s/step). The mineralogical interpretation was done using the software X'Pert HighScore, installed on the X-ray diffractometer.

3.2.3. Mössbauer Spectroscopy
Mössbauer spectroscopy allows, by studying the hyperfine parameters, the identification of different Fe-bearing phases, the quantification of their relative fractions in solid samples, and the determination of the oxidation state of Fe in each phase [*Vandenberghe*, 1991; *Murad*, 2010]. Mössbauer spectra of volcanic materials were taken at room temperature (RT), with a 512-channel conventional spectrometer at constant acceleration and a source of ^{57}CoRh with a nominal activity of approximately 10 mCi. Velocity calibration was performed at RT with a 12 μm thick α-Fe foil. The Mössbauer spectra were numerically analyzed using quadrupole splitting distributions. The oxidation state of Fe (Table 2) was determined by analyzing the magnitude of the obtained isomeric shifts [*Murad*, 2010].

3.2.4. Electron Microprobe Analysis
Ash samples were mounted on a stub and carbon coated in order to be studied in a JEOL-JXA 8230 electron microprobe equipped with an energy-dispersive detector (EDS) for semiquantitative chemical analysis. In order to investigate the chemical composition of glass shards and other inorganic phases, samples were carefully examined for morphological features and semiquantitative analysis using different magnifications. As the same group of Patagonian ash samples were also studied to define the solid speciation of As, related scanning electron microscopy (SEM)/EDS data can be viewed in detail at *Bia et al.* [2015].

3.2.5. Solubility of Fe in Volcanic Ashes
The solubility of Fe from volcanic ash was studied by two different methods: a continuous flow method and leaching experiments using seawater.

A continuous flow method (CF) has been optimized and validated as applied to tiny amounts of atmospheric dust/ash samples (see details in *Simonella et al.* [2014]). Briefly, both a blank extraction solution and a flow extraction solution in triplicate are carried out simultaneously. The solution extraction stream is propelled by a peristaltic pump (Gilson Minipuls 3®) at 0.98 mL min^{-1}. It passes through a column that contains an accurately weighed sample (~5 mg). Aliquots of emerging solution (~200 μL) are collected in PTFE (Teflon) wells, which are placed in the autosampler of a graphite furnace atomic absorption spectrometer (GFAAS). The experiment consists of two steps; first, a flow of deionized water (DI) (MilliQ, pH ~ 5 and 18 mΩ cm^{-1}) passes through the column for 20 min. DI extraction is intended to measure readily extracted (potentially bioavailable) surface phases. It was observed that 20 min were enough for removing the easily
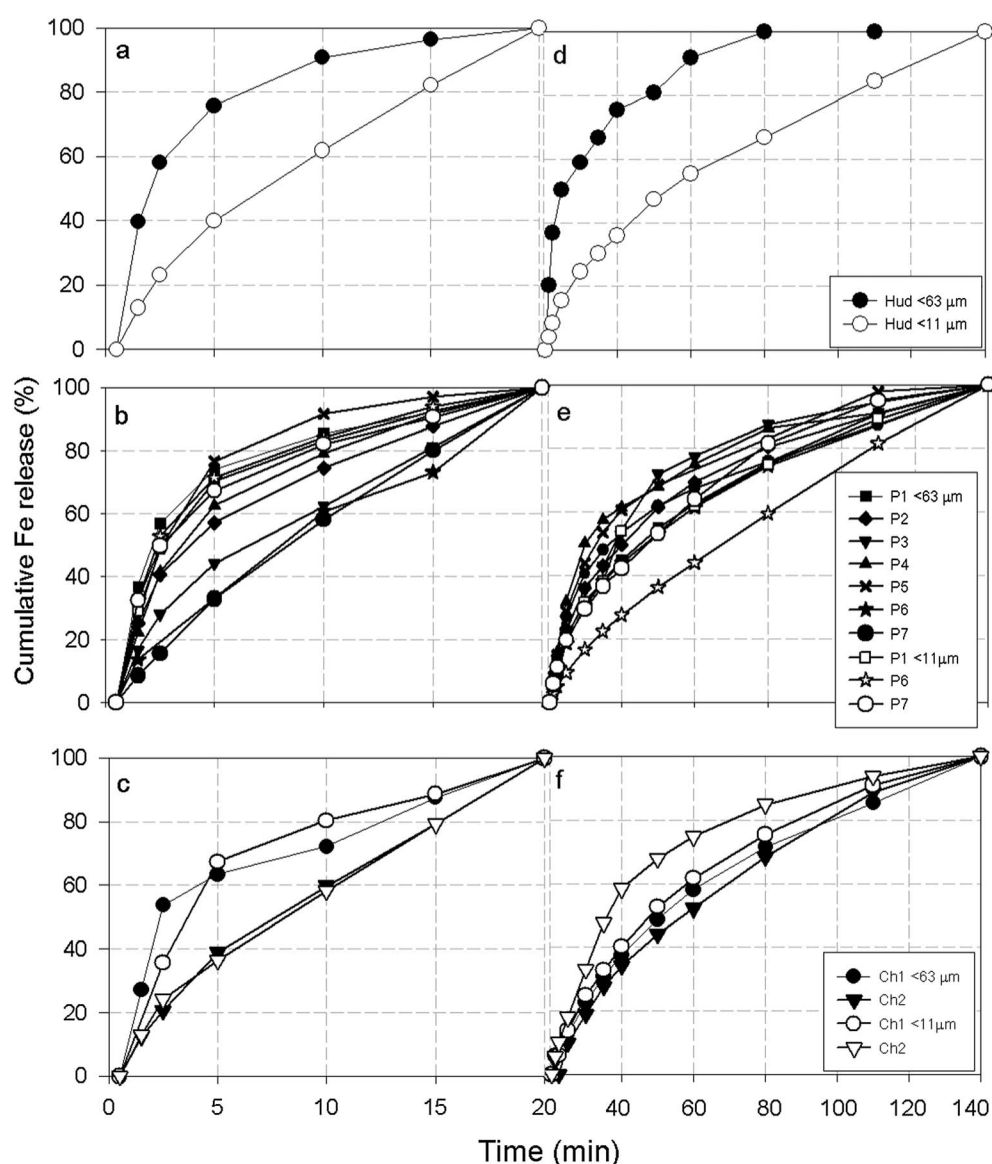
Figure 1. Iron release from Patagonian volcanic ashes. (a–c) Percent of the total Fe released using deionized water (Fe_{DI}); (d–f) Percent of the total Fe released using 1% vol/vol of HNO_3 (Fe_{WA}). Black and white symbols represent $< 63\,\mu m$ and $< 11\,\mu m$ grain size fractions, respectively.

available Fe (hereafter Fe_{DI}) from sediment/ash [*Simonella et al.*, 2014]. During this time, eight aliquots of $200\,\mu L$ are taken from the output of the system. Fe_{DI} data in Table 2 represent the cumulative values for the eight samples collected over 20 min that are shown in Figure 1. The second step consists of extraction with a diluted acid solution (WA, 1% HNO_3; pH ~ 2.0) which passes through the system for 120 min. This is intended to measure Fe in surface or bulk mineral phases that are insoluble in DI (hereafter Fe_{WA}). For most of the samples, we observed a fast Fe release after 30–40 min of sediment/ash contact with HNO_3 1%. Afterward, the dissolved Fe concentration increases at a slower rate. In this case, 12 aliquots of solution were collected from the end of the system. Cumulative values for the 12 samples collected over 120 min are shown in Table 2 and Figure 1. Several studies have determined the solubility of Fe from minerals found in atmospheric dusts using an acid solution [e.g., *Journet et al.*, 2008; *Shi et al.*, 2011]. The rationale for this is that an important chemical change during atmospheric processing is the change of pH in the water droplets surrounding airborne particles. In the atmosphere, the presence of SO_x and NO_x gases can be formed as a result of pollution and/or from natural processes. As the water

droplets become saturated with CO_2, these gases will dissolve decreasing the pH of the water droplets [e.g., *Shi et al.*, 2011]. According to thermodynamic modeling a pH of 2 or lower is often expected in the airborne particle surface due to coating of HNO_3 and H_2SO_4 [*Meskhidze et al.*, 2003; *Chate and Devara*, 2009; *Nenes et al.*, 2011; *He et al.*, 2012]. Furthermore, during atmospheric transport of mineral dust or volcanic ash particles, clouds repeatedly evaporate, leaving a thin film of aqueous electrolyte surrounding particles. Compared to a cloud droplet, this aqueous film is very acidic and can reach pH values of 2 or even lower [*Solmon et al.*, 2009]. Due to multiple series of development and evaporation of clouds, 5 to 10 cycles of pH alternation in the aqueous film around mineral dust/volcanic ash particles can occur before these particles are deposited via wet deposition [*Seinfeld and Pandis*, 2006; *Baker and Croot*, 2010]. Then, low pH conditions of the aqueous film surrounding ash particles can promote acid leaching and dissolution of Fe-bearing phases that can have potential consequences for the ash Fe solubility in seawater [*Ayris and Delmelle*, 2012].

Surface seawater was collected near the Patagonian coast at Puerto Pirámides (42°39′S; 64°14′W, a small village ~100 km north from the city of Trelew). The samples were filtered in situ with 0.45 μm membranes and stored at 4°C in acid-cleaned dark polyethylene bottles. This extraction is aimed at measuring the iron that could be bioavailable in seawater (Fe_{sw}). For these experiments approximately 10 mg of ash was added to 20 mL of seawater. Measurements were performed every few minutes using cathodic stripping voltammetry under clean laboratory conditions (as described in *Croot and Johansson* [2000]). Cumulative values of these measurements (Fe_{SW}) can be seen in Table 2. This experimental setup intends to mimic the soluble Fe input from volcanic ash and mineral dust into seawater through dry deposition [*Duggen et al.*, 2007; *Olgun et al.*, 2011], which is considered the globally dominant deposition process for atmospheric particles [*Jickells and Spokes*, 2001].

3.2.6. Chemical Analysis

Dissolved Fe concentrations were measured by using flame atomic absorption spectrometer (FAAS) equipped with a deuterium background corrector and graphite furnace atomic absorption spectrometer (GFAAS). In order to evaluate the standard method of extraction and the GFAAS measurements, the procedure was applied to a certified reference material (BCR-701, certified by the Community Bureau of Reference). Results varied between ±6% in relation to certified values for the different stages of extraction (see details in *Simonella et al.* [2014]).

Major elements in ashes were analyzed at a commercial lab (Actlabs, Canada). Fused beads, prepared at 1050°C using $Li_2B_4O_7$, were digested with HNO_3 and analyzed by inductively coupled plasma optical spectrometry (detection limit = 0.01% and 2% uncertainty based on one relative standard deviation of replicates). The validity of the results was checked with NIST 694, 696, and 1633b, which were carried out along with sample analysis. The pH and the specific conductivity were measured in batches of water/ash leachates immediately after ash-water mixing (100 mg ash in 40 mL of DI water).

3.2.7. Model Simulation of Ash Deposition Over the Ocean

The Hybrid Single-Particle Lagrangian Integrated Trajectory (HYSPLIT) model [*Draxler and Hess*, 1998] has been configured to simulate the Puyehue volcano eruption by assuming that the ash emission can be represented by a vertical line source, with ash distributed uniformly from the volcano summit to the top of the volcano eruption column [*Stunder et al.*, 2007]. The source term is based on an empirical formula that relates the height of the eruption column to the mass eruption rate [*Mastin et al.*, 2009a, 2009b]. The height of the eruption column is estimated from *Collini et al.* [2013]. In this work, we assume a particle distribution based on four size bins [*Heffter and Stunder*, 1993]. Given a particle diameter, density, and shape factor, the model can estimate gravitational settling along with wet deposition [*Draxler and Hess*, 1998]. HYSPLIT is driven by meteorological fields from the National Centers for Environmental Prediction's Global Data Assimilation Scheme at 1 × 1° resolution [*Kanamitsu*, 1989; *Kalnay et al.*, 1996].

4. Results and Discussions

4.1. Chemical and Mineralogical Composition of Patagonian Ashes

The magma source is probably one of the main factors controlling the release of metal from volcanic ash [*Armienta et al.*, 2002]. The Patagonian ashes have different bulk geochemical composition, including andesite (Hudson), trachydacite (Puyehue), and rhyolite (Chaitén). The total Fe content reflects the type of

Table 3. Mineralogical Composition of Patagonian Ash, Topsoil, and Dust Samples[a]

Sample ID	Percent Modal Composition[b]			Mineral Composition (XRD)						
	Glass	Minerals	Opaque Minerals	Qz	Pg	Cr	Cal	Gy	Ha	CM
P1	88	10	2.2	*	***	nd	nd	nd	nd	nd
P2	90	9	1.0	*	***	nd	nd	nd	nd	nd
P3	98	1	0.6	nd	***	nd	nd	nd	nd	nd
P4	87	12	0.7	**	**	nd	*	nd	nd	nd
P5	77	21	2.3	**	*	nd	*	*	*	*
P6	90	9	0.6	*	***	nd	*	nd	nd	**
P7	90	9	1.0	*	***	nd	nd	nd	nd	**
HUD	85	12	2.9	nd	***	nd	nd	nd	nd	nd
CH1	76	21	2.4	*	***	*	nd	nd	nd	nd
CH2	87	12	1.0	*	***	*	nd	nd	nd	nd
TS1	na	na	na	*	*	nd	*	*	*	**
TS2	na	na	na	*	*	nd	*	nd	nd	**
Tw-dust	na	na	na	**	**	nd	*	nd	*	**

[a]All samples were analyzed in the <63 μm grain size fraction. Qz, quartz; Pg, plagioclase; Cr, cristobalite; Cal, calcite; Gy, gypsum; Ha, halite; CM, clay minerals; nd; not detected, and na; not available: *, scarce; **, frequent; and ***, common.
[b]Optical microscopy.

magma from which they are derived [e.g., *Rogers and Hawkesworth*, 2000]. For the case of Patagonian ashes, low total Fe_2O_3 content (<2%) and high total SiO_2 (>72%) characterize the Chaitén ashes, while high total Fe_2O_3 content (>6%) and low total SiO_2 content (<61%) characterize the Hudson ashes. Intermediate values are observed for the Puyehue ashes (~4–5% of Fe_2O_3 and 66 to 70% of SiO_2) (Table 2).

The mineralogical composition of the studied ashes is dominated by volcanic glasses (76 to 98%), with subordinate amounts of crystalline materials (2 to 24%) (Table 3). These results agree with previous data reported by the Global Volcanism Program (http://www.volcano.si.edu/world/volcano.cfm?vnum=1508-057&volpage=var#bgvn_2002).

Table 3 shows that vitric particles (~85%) dominate the Hudson sample (Hud). About 12% of the Hudson ash is represented by birefringent (mainly plagioclase) and ~3% of opaque minerals. SEM/EDS analyses revealed the presence of primary minerals such as magnetite, amphibole, pyroxene, ilmenite, and pyrite, along with some coatings and individual crystals of salts (mainly Fe sulfate, halite, calcite, and gypsum) (Figure 2). Besides, *Bia et al.* [2015] identified Ti and Fe (hydr)oxide coatings associated with pyroxene and plagioclase.

For the Chaitén ashes (Ch1 and Ch2), relatively more birefringent phases (12 to 21%) can be identified, represented mainly by plagioclase, with a scarce presence of quartz and cristobalite. SEM/EDS analyses reveal the presence of Fe and Mn oxides, ilmenite, olivine, euhedral pyrite, and amorphous Fe-S coatings, probably Fe sulfate [*Bia et al.*, 2015] in scarce proportions, which is in agreement with the 1–2% amount of opaque minerals observed through point counting of loose grains (Table 3). Other studies also indicate the presence of ilmenite, magnetite, and orthopyroxenes [*Castro and Dingwell*, 2009].

Glass shards (87–98%) are also the main mineralogical components for the Puyehue ashes (P1–P7). Here birefringent minerals range between 1 and 10% and are mainly represented by plagioclases and scarce presence of quartz. Opaque crystalline phases ranged between 0.6 and 2.2%. The CNEA (Comisión Nacional de Energía Atómica, 2011, http://cab.cnea.gov.ar/noticiasanteriores/erupcionCaulle2011/informeGeneralFinal.pdf) also observed the presence of pyroxenes and a very scarce amount of ilmenite. Micro-Raman spectroscopy detected a complex mineralogical mixture dispersed in the glassy matrix, basically formed by alkali aluminosilicate, hematite, and magnetite [*Botto et al.*, 2013]. Minor presence of gypsum (Figure 2c) and Fe (hydr)oxides was also identified by EDS mapping. For samples P4 and P5, an increased amount of quartz, trace of calcite, and gypsum and the frequent presence of clay minerals (e.g., sample P5) is observed. As highlighted in the following paragraphs, many clues indicate that the Cutral-Có (P4) and General Roca (P5) samples were contaminated with local dust. Important strong winds occurred during the volcanic eruption, thus affecting ash deposits and promoting the resuspension and remobilization of volcanic material [*Collini et al.*, 2013]. Although these samples are not regarded as representative of pristine
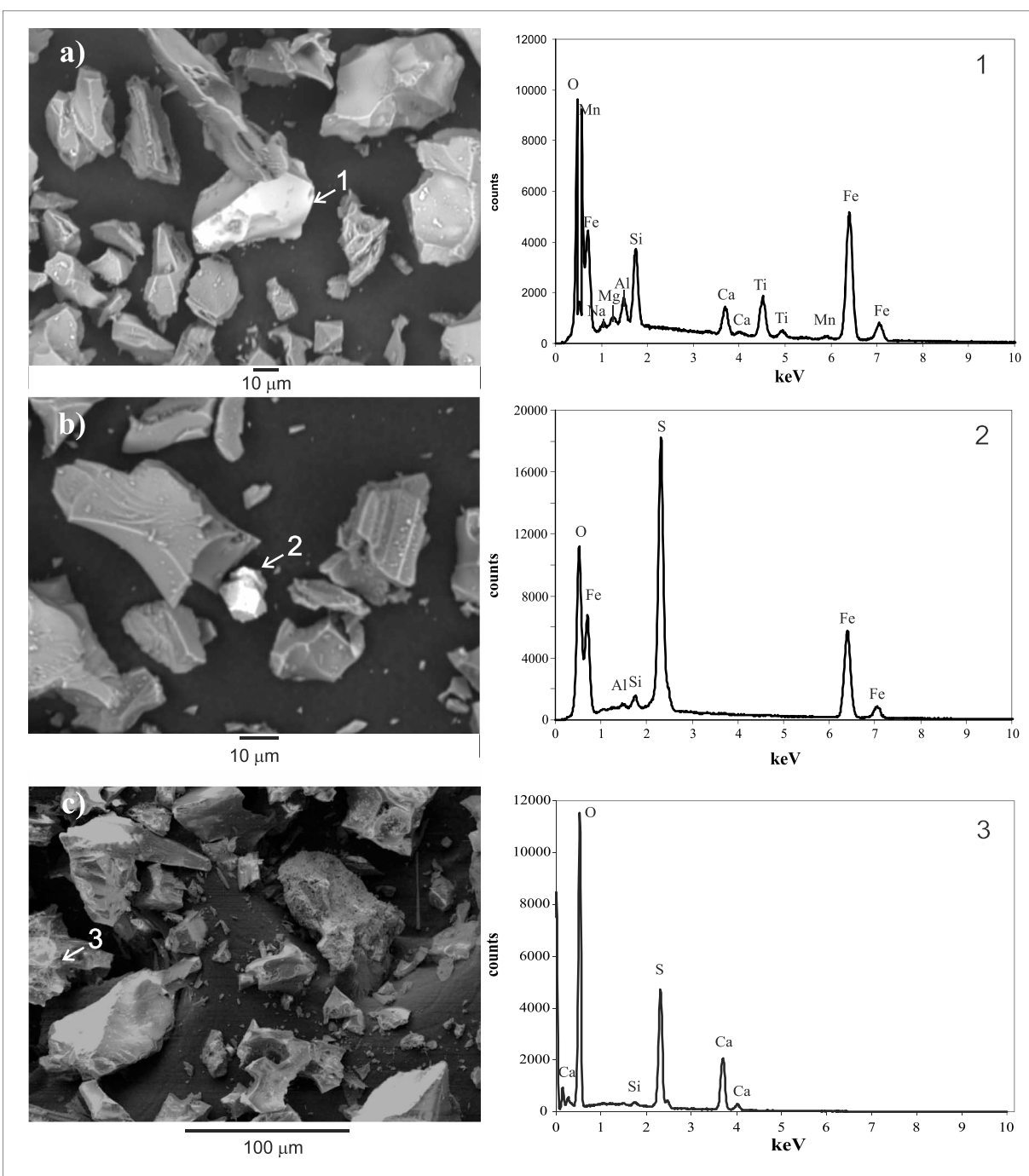
Figure 2. Fe-bearing minerals and salts identified in Patagonian ashes by SEM/EDS analysis: (a) Hudson, coatings of Fe/Mn oxides onto aluminosilicate glass. (b) Hudson, subheudral grain of Fe sulphate. (c) Puyehue, coatings of anhidrite.

conditions, they are useful in investigating a widespread effect after volcanic eruptions, as they represent the atmospheric transport of mixed ashes with Patagonian dust.

Summarizing, the mineralogy of ashes is dominated by glass with minor presence of birefringent phases. Except for the Chaitén, SEM/EDS analyses permitted to observe the presence of salts (e.g., gypsum and halite). In the three types of ashes the more abundant crystalline Fe-bearing phases were hematite, magnetite, and ilmenite, while pyrite and Fe sulfates were observed only in the Hudson and Chaitén samples [*Bia et al.*, 2015].
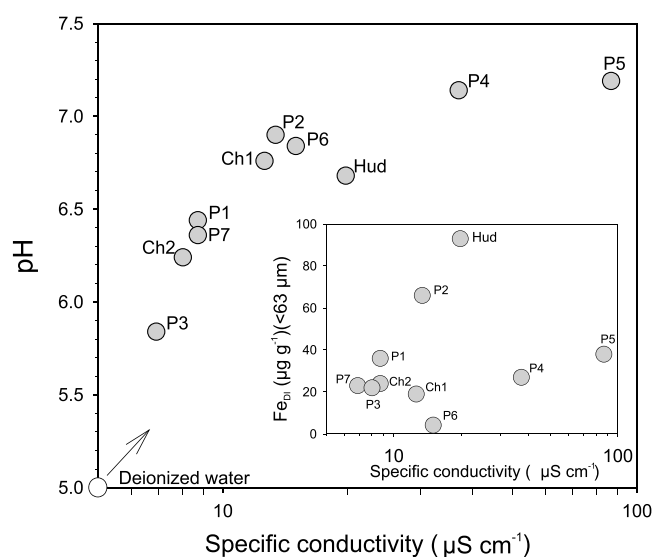
Figure 3. Measurement of pH and specific conductivity (approximately total dissolved solids) after ash contact with deionized water. Insert shows strong correlation between dissolved Fe extracted using deionized water (Fe_{DI}) and the specific conductivity. A lower slope correlation is observed for ash samples contaminated with surface soils.

4.2. Soluble Fe in Patagonian Ashes
4.2.1. Release of Fe in Deionized Water

The cumulative percentage of Fe released from suspensions in deionized water (e.g., cumulative Fe concentrations compared to bulk) shows lower values for Puyehue (mean = 0.07%) and is about 2 times higher (0.10–0.15%) for Chaitén and Hudson ashes. In general, the amount of Fe released in deionized water from Patagonian dust and topsoil samples was relatively lower (<0.1%), and these values are in the range of data reported for similar experiments carried out with suspensions of arid soils [*Schroth et al.*, 2009].

The release of Fe_{DI} showed different trends according to the evaluated grain size fraction. Puyehue ashes release higher concentrations 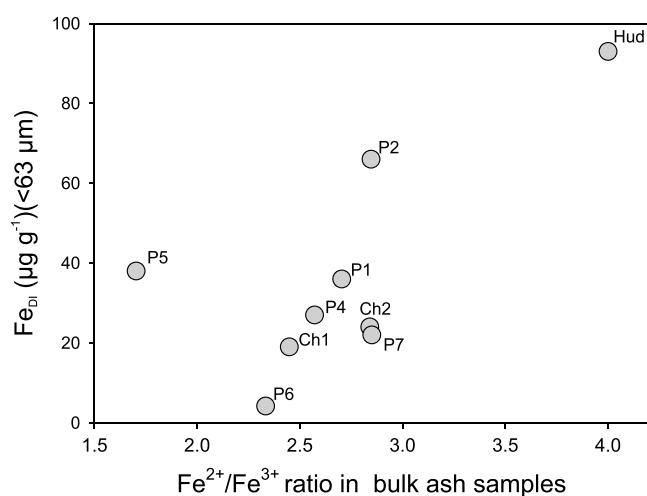of Fe_{DI} in suspensions prepared with the finer grain size fraction, while the opposite trend is observed for the Hudson ash suspensions. The Chaitén samples release similar amounts of Fe_{DI} regardless of grain size fraction.

The fastest liberation rate is observed for the <63 μm fraction of Hudson ash (Figure 1a). In general, similar rates of Fe_{DI} release are observed for both grain size fractions in the Chaitén and Puyehue samples (Figures 1b and 1c), suggesting that similar phases could contribute Fe independently of grain size. On the other hand, the Hudson ash shows a faster Fe liberation in the coarse grain size fraction and suggests that different phases could contribute to the pool of soluble Fe measured in this sample. This characteristic is not evident in the other samples, where the rate of Fe release does not show a clear control with particle grain size.

Deionized water has no buffering capacity, and it can primarily leach the easily soluble salts absorbed on ash surfaces [e.g., *Ruggieri et al.*, 2012; *Witham et al.*, 2005]. Accordingly, Figure 3 indicates that the interaction between volcanic ash and deionized water (pH ~ 5.0) increased the solution pH from slightly acid to neutral or weakly alkaline and that pH correlates significantly with the increase of the specific conductivity (SC, i.e., approximately total dissolved solid). The straight part of this correlation is probably the consequence of the rapid dissolution of alkaline compounds and the release into solution of hydroxyl ions from oxogroups present on the particle ash surface [e.g., *Toscano et al.*, 2008; *Ruggieri et al.*, 2012]. *Olsson et al.* [2013] observed for similar experiments that dissolution of nonsilicate phases dominated during the first 10 min of ash-water interactions. After this time, dissolution of silicate phases could explain the increase on alkalinity and the consumption of protons. In Puyehue samples P4, P5, and to a lesser extent P6, Fe_{DI} release is relatively low. In these samples the dissolution of minerals such as calcite, gypsum, and halite (Figure 2 and Table 3) could promote the consumption of H^+ leading to increasing pH and SC values. Under alkaline conditions, Fe probably precipitates in the form of Fe (hydro)oxide phases or Si-Al-Fe surface gels [e.g., *Olsson et al.*, 2014] (Figure 3 insert).

The ratio Fe^{2+}/Fe^{3+} in the ash samples was determined by hyperfine analysis of Mössbauer spectra. The obtained results indicate that there is a strong dependence of Fe_{DI} with increasing Fe^{2+}/Fe^{3+} ratios (Figure 4). As ferrous salts are more soluble than Fe^{3+} salts [*Ayris and Delmelle*, 2012; *Delmelle et al.*, 2007], this trend indicates that the amount of Fe released in DI is mostly due to the dissolution of Fe(II) phases present in the form of thin coatings. These coatings were detected by X-ray photoelectron spectroscopy (XPS) analysis in a related work on the same Patagonian ashes [*Bia et al.*, 2015]. The presence of nonmagmatic minerals in volcanic ash could explain the offset position of sample P5 (see Table 2).

Figure 4. Dependence of Fe extracted using deionized water (Fe_{DI}) with the total Fe^{2+}/Fe^{3+} species abundances in volcanic ashes.

In basic ashes like Hudson, high Fe_{DI} values could be associated with the generation of acidic conditions due to acid gas condensation onto ash particles within the volcanic plume [*Gislason et al.*, 2011]. Salts containing soluble ferric and/or ferrous iron species (e.g., Fe sulfate; see Figure 2b) can coat the surface of ash grains as a product of the interaction between gas, aerosol, and ash particles within the eruption plume. The Hudson ash shows Fe_{DI} release levels on the same order of magnitude as those found by *Jones and Gislason* [2008] for the basic Hekla ash. Similar to Hekla, the high Fe_{DI} release from Hudson ash could be associated with the combination of strong acidity and high fluoride concentration in the eruption plume, which would permit the presence of readily soluble Fe-bearing phases [*Jones and Gislason*, 2008]. Also similar to Hekla, Hudson ash has coarse grain size mode, pointing out that high Fe_{DI} release from this material is not associated with a particle size effect but probably to increased surface area due to acidic conditions [e.g., *Ayris and Delmelle*, 2012]. Batch experiments conducted by *Ruggieri et al.* [2010] found that fluoride released from Hudson ash is over 20 times higher than in the Chaitén ash. *Durant et al.* [2012] also found that a very small amount of Fe is released from Chaitén ashes after DI water treatment, suggesting that minimal amounts of acid were adsorbed onto the Chaitén ash particle surface. Compared to the Hudson ashes, results suggest that the Chaitén ashes were less affected by acid leaching during the plume process. This explains why, in general, in deionized water, a more limited release of Fe-bearing phases occurs at a slower rate of liberation (Table 2 and Figure 1c).

From the above discussion we conclude that grain size of particles appears as a secondary factor controlling Fe_{DI} in Patagonian ashes. The amount and rate of Fe_{DI} released from these ashes seem to be mainly controlled by the relative abundance of surface ferrous soluble salts, whose presence seems to be associated to the acid conditions predominating in the volcanic plume.

4.2.2. Release of Fe in Weak Acid Solution

Low pH values are expected during the volcanic ash plume process [*Ayris and Delmelle*, 2012]. Experiments run to decipher the main phases contributing nutrients from volcanic ash under acidic condition are contradictory. For example, *Hamilton and Pantano* [2000] found that at pH 2, the dissolution rates of plagioclase and glass are almost the same. On the other hand, *Wolff-Boenisch et al.* [2006] found that at pH 4, dissolution rates of both minerals and glasses decrease with an increasing Si:O ratio but that glass dissolution rate is faster than corresponding mineral rates.

Probably due to a bulk effect, data indicate that the higher presence of glass in volcanic ash samples promotes lower Fe_{WA} release. Figure 5 suggests that the amount of Fe_{WA} released from Patagonian ashes is probably associated with the fine crystalline components of these materials. The maximum extraction of Fe_{WA} corresponds to Chaitén samples, which have higher contents of crystalline minerals and a finer grain size mode. On the contrary, when ashes are composed almost exclusively of glass shards (~98%) and have coarse grain size mode (42 μm), little Fe_{WA} is released (e.g., sample P3). Semiquantitative estimations indicate that plagioclase and, to a lesser extent, quartz are the dominant birefringent phases, representing ~90% of the total crystalline minerals. Although estimates should be taken with cautions [*Raiswell and Canfield*, 2012], at pH 2 the solubility of plagioclase is about 4 times higher than Fe oxides (e.g., magnetite) [*Journet et al.*, 2008]. The contents of Fe in plagioclase are 0.12 wt % in Chaitén ash [*Castro and Dingwell*, 2009] and 0.44 wt % in Hudson ash [*Kratzmann et al.*, 2009]. Based on the solubility data reported by *Journet et al.* [2008] and assuming that plagioclase is the only birefringent phase, we estimate that less than 10% of the dissolved Fe released into a weak acid medium can be contributed by this mineral.
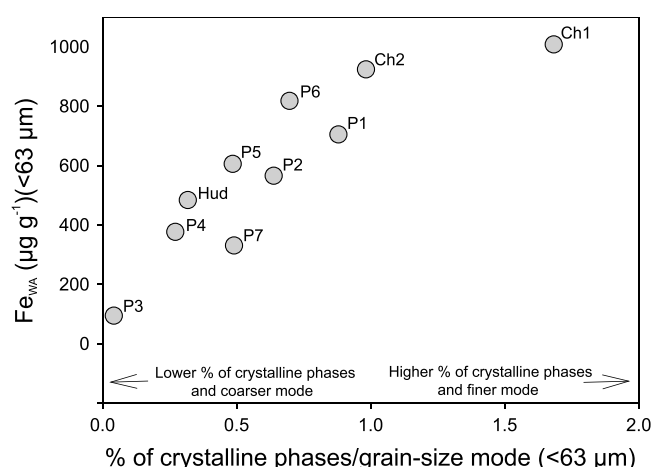
Figure 5. Dependence of Fe released using 1% vol/vol of HNO_3 (Fe_{WA}) with the relative abundance of crystalline phases and the dominant grain size mode of volcanic ashes.

Table 3 shows that opaque minerals, present in a range of 0.5 to 3%, are the main Fe-rich minerals, represented mainly by magnetite and ilmenite. The dissolution rate of magnetite is very low [*Journet et al.*, 2008], and according to XDR and magnetic analyses, the amount of this mineral in Patagonian ashes is <1%, suggesting little contribution to the bulk of Fe_{WA} concentrations. Although the amounts of TiO_2 in ashes significantly correlate with total Fe_2O_3 concentration ($r^2 = 0.888$; $p > 0.05$), an opposite trend is observed when TiO_2 concentrations are contrasted against Fe_{WA} values. This observation suggests that there is no important Fe contribution from ilmenite under acidic conditions.

A significant amount of Fe released under weak acid conditions must therefore have originated from phases other than primary minerals or glasses. For the three types of ashes, X-ray photoelectron spectroscopy (XPS) suggested the presence of thin coatings of Fe (hydr)oxides. These data also indicate that Fe is depleted in the surface of particles compared to the bulk Fe concentration for Hudson and Puyehue materials but have similar concentrations for the Chaitén ash [*Bia et al.*, 2015]. Moreover, *Ayris and Delmelle* [2012] found the existence of a strong Fe enrichment on the surface of samples from the Chaitén. Along these lines, *Durant et al.* [2012] observed a sugary appearance on Chaitén ash particles due to coatings of very small grains.

We propose that apart from the contributions from glass and minerals, a high proportion of Fe extracted after weak acid treatment reflects the enrichment of Fe in water-insoluble coatings developed on fine ash particles. Further studies should evaluate the possibility that during the previous contact of ash with deionized water, precipitation of secondary Fe phases could have occurred. On the other hand, lower Fe_{WA} values could indicate Fe depletion on the surface of particles, due to acid leaching during interaction with the volcanic gas/aerosol phase, as was similarly observed in Hekla ash, Iceland [*Delmelle et al.*, 2007; *Ayris and Delmelle*, 2012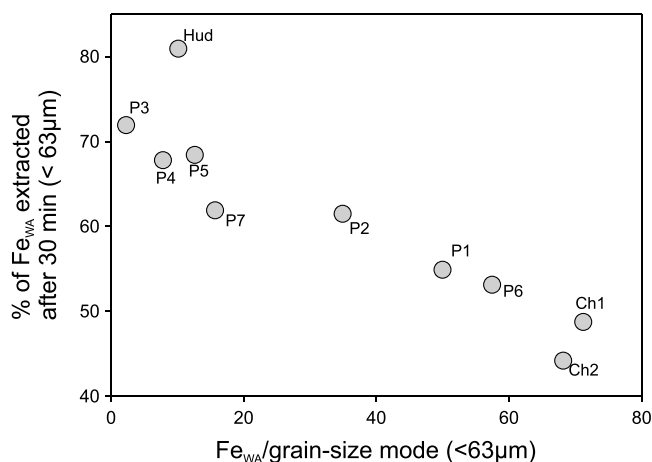], and in some of the Patagonian ash samples studied here. Furthermore, Figure 6 suggests that the liberation rate and the total amount of Fe released under acidic conditions are controlled by grain size, amount of crystalline phases, and in-plume processes of each type of volcanic material. Here the highest Fe_{WA} release and the slowest rate were determined for the Chaitén ash, which accounts for the dominance of small particles that probably were less affected by acidic conditions within the eruption plume. The almost exclusive presence of glass shards seems to avoid a significant presence of oxyhydroxide Fe-bearing precipitates (e.g., sample P3), or at a minimum, these phases were less developed under acidic conditions during plume process (e.g., Hudson).
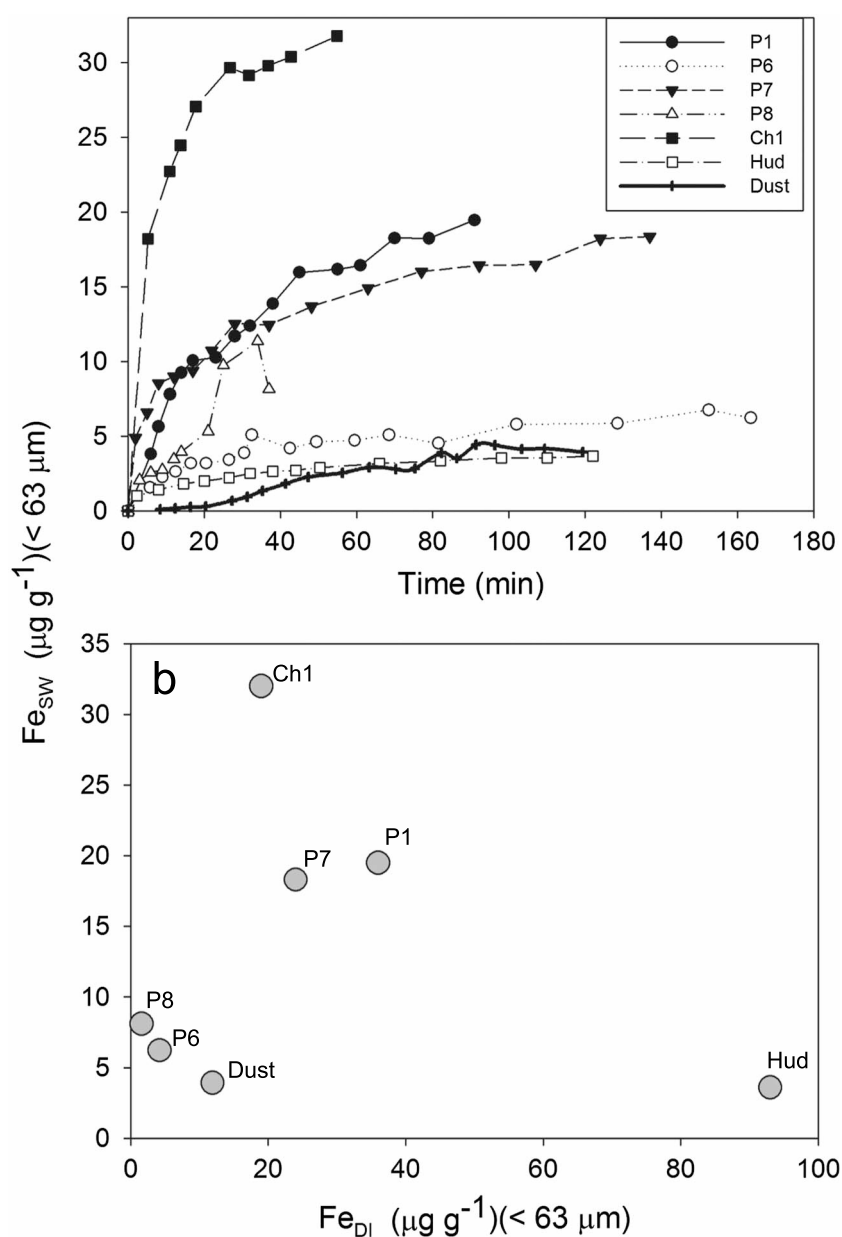

Figure 6. The rate of dissolution of Fe extracted with weak acid (Fe_{WA}) is lower when ash samples are dominated by small particles and are less affected by acidic conditions during the plume process (Ch1 and Ch2). Faster dissolution rates are observed when the mineralogical composition of the samples is dominated by glass shards (P3) or because these precipitates are less developed due to acidic conditions during the eruption plume (Hud).

Figure 7. (a) Dissolution rate of Fe from ash sample treated with seawater (Fe_{SW}). (b) Comparative soluble Fe concentrations obtained after treatment with deionized water (Fe_{DI}-CF method) and batch experiment using seawater (Fe_{SW}) for the same volcanic ash samples.

For the <11 μm grain size fractions, most of the ash samples show similar Fe_{WA} liberation rates compared to the coarse fraction (except Hudson, Table 2). This observation also supports the idea that apart from the mineralogy, a higher specific surface area in finer volcanic ashes is an important factor which can explain the increase in Fe solubility under acidic conditions.

4.2.3. Solubility of Fe in Seawater

Concurring with the range obtained for ash samples from subduction zones and hot spot volcanoes [*Olgun et al.*, 2011], Patagonian volcanic ashes release between 3.0 and 30 μg g^{-1} of Fe after contact with seawater (Fe_{SW}) (Table 2). Figure 7a shows that the kinetic Fe_{SW} release data agree with the previous experiment performed with ash and seawater [*Duggen et al.*, 2007; *Jones and Gislason*, 2008; *Olgun et al.*, 2011; *Frogner et al.*, 2001], indicating that Fe release from Patagonian ashes occurred within ~40 min of contact with seawater, relatively slower compared to the velocity of Fe released using deionized water. In
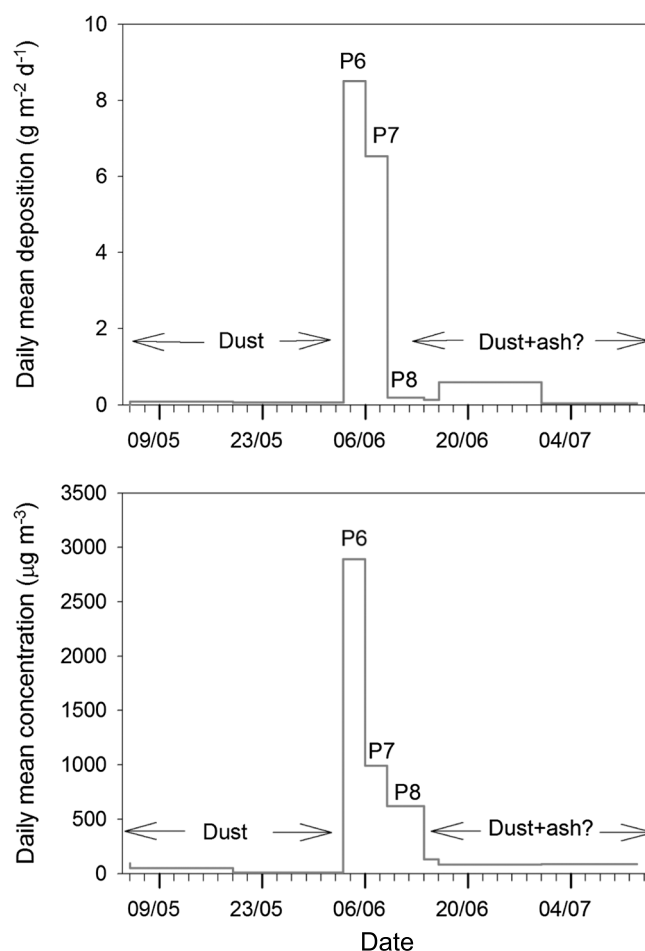
Figure 8. Mean daily deposition and concentration of volcanic ash measured at Trelew monitoring station between 4 and 14 June 2011. The high deposition/concentration of ash contrasts with background dust recorded at the same monitoring site.

seawater,the extent of Fe dissolution is governed by the pH and, compared to deionized water experiments, these studies will always have much smaller apparent fractional solubilities unless there is a chelator present to take up the iron dissolving and prevent it from precipitating [*Baker and Croot*, 2010]; this is what also causes the apparent slower kinetics of release [*Croot and Heller*, 2012].

The fastest Fe_{SW} release rate is observed in the Chaitén sample, while the Hudson sample exhibits the lowest rate. Puyehue materials show intermediate values (Figures 7a and 7b). Higher Fe_{SW} values for Chaitén ash were also observed in a similar study performed by *Olgun et al.* [2011], which may reflect Fe enrichment at the ash particle surface [*Durant et al.*, 2012]. Data also indicate that higher Fe_{SW} solubility values were found in samples with low Fe_{DI} solubility concentrations (e.g., Chaitén ash). Similar experiments concluded that the very rapid release of Fe_{SW} (minute to hour scale) is most likely dominated by fast dissolution of the surface salts rather than dissolution of glass particles [e.g., *Duggen et al.*, 2007; *Frogner et al.*, 2001; *Jones and Gislason*, 2008]. Our data also suggest that rhyolitic eruptions produce Fe-bearing salts that are more soluble in

seawater than volcanic material derived from andesitic composition (e.g., Hudson ash; Figure 7b). As was also observed in the Hekla ash [*Olgun et al.*, 2011; *Jones and Gislason*, 2008], the Hudson ash shows that the total Fe dissolved in seawater has a lower concentration compared to data obtained by means of continuous flow experiments using deionized water (Fe_{DI}). Notably, data from Hudson ash indicate that batch experiments using acetic acid and seawater solvents obtained similar low dissolved Fe concentrations [*Simonella et al.*, 2014]. In the Hudson ash, increasing acidic conditions seems to decrease the solubility of compounds containing Fe. There, the higher buffering capacity of seawater could most likely prevent acidic conditions, avoiding Fe solubility of basic ashes.

Compared to ash samples, the Trelew dust storm sample depicts slower Fe_{SW} liberation rates and concentrations, similar to those found by other experiments performed with dust and seawater [e.g., *Spokes and Jickells*, 1996; *Olgun et al.*, 2011]. Iron release values for this sample are similar to values found in samples P6 and P8, reinforcing the idea that ash samples collected at the monitoring site could have been contaminated with Patagonian dust.

4.3. Soluble Fe-Ash Inputs to the Southern Ocean: The Puyehue Eruption Case Study

Figure 8 shows dust/ash fluxes and concentration for before, during, and after the eruption of the Puyehue volcano. It is noteworthy that for the first time, the Trelew monitoring station has recorded and obtained ash samples of the entire eruption of a southern Andean volcano. Flux data indicate that after 14 June 2011, ash concentrations dropped dramatically, almost reaching the dust background values observed

Table 4. Measured and Modeled Ash Deposition/Concentration of Puyehue Volcanic Eruption at Trelew[a]

ID	Sampling Period					Measured Deposition $(g\,m^{-2}\,d^{-1})$	Model Deposition $(g\,m^{-2}\,d^{-1})$	Measured Concentration $(\mu g\,m^{-3})$	Model Concentration $(\mu g\,m^{-3})$
	Start Date	Local Time	End Date	Local Time	Days				
P6	3 June 2011	17:00	6 June 11	16:00	2[b]	8.5	0.0	2890	28
P7	6 June 2011	17:00	9 June 2011	17:00	3	6.5	5.3	991	2938
P8	9 June 2011	18:00	14 June 2011	15:30	5	0.2	6.5	621	217
Dust	5 August 2009		28 July 2011		723[c]	0.072 (0.001–0.16)[d]		18.5 (0.11–132)[d]	

[a]For comparison, a 2 year based mean dust deposition/concentration at the same site is shown.
[b]Assuming 4 June as the beginning of the eruption; see text.
[c]Samples were collected approximately every 14 days, given a total of 52 observations.
[d]Deposition range.

previous to the eruption. Due to wind ash remobilization, the dust background concentration was clearly modified after the end of the main eruption phase. Table 4 indicates that maximum concentrations were recorded during 4–6 June ($>2800\,\mu g\,m^{-3}$, sample P6). Mean daily ash concentration during the entire eruption period exceeded $1500\,\mu g\,m^{-3}$, similar to the maximum daily average concentration recorded during the eruption of Eyjafjajllajökull, Iceland [*Thorsteinsson et al.*, 2012]. Comparatively, a 2 year based measurement of dust concentration at Trelew indicates a mean daily value of $18.5\,\mu g\,m^{-3}$ and concentrations of over $130\,\mu g\,m^{-3}$ for periods when dust storms occurred (Table 4). Similarly, the daily horizontal dust fluxes (emission) measured at Trelew are $\sim11\,g\,m^{-2}$ (not shown), equivalent to $\sim4000\,g\,m^{-2}\,yr$. The net emission of ash measured at Trelew indicates that over the course of 10 days, $\sim1900\,g\,m^{-2}$ of volcanic material was exported to the ocean. This amount is equal to more than half of the yearly flux typically contributed by dust.

Compared to experimental data, the HYSPLIT model at Trelew estimates a similar mean daily value ($\sim1100\,\mu g\,m^{-3}$); inconsistencies, however, are evident when data from the different periods are compared (Table 4). A comparison with visible satellite images (MODIS, http://lance-modis.eosdis.nasa.gov) (not shown) indicates that the model captures the geographical extent and timing of the ash vertical column. Although this is a necessary condition in order to gain confidence in the ability of the model to depict the vertically integrated column, it is not sufficient to determine the vertical distribution of the aerosols. As a consequence, we compared the particulate matter surface concentrations measured at the Trelew site with the simulated values. Overall, considering the entire duration of the eruption period (4–20 June, according to *Collini et al.* [2013]), the model captures the magnitude of the particulate matter concentrations measured at the Trelew station. However, the simulation grossly underestimates values for the P6 period. This is mainly due to suppression in the vertical mixing that produces a delay in the plume touchdown over the site. In order to further investigate this issue, we used the Weather Research and Forecast [*Skamarock et al.*, 2008], with a horizontal resolution of 12 km to drive HYSPLIT. However, even with this higher resolution, the model was not able to mix down the ash plume at the right time. Consequently, at the beginning of the next sampling period (P7), the model seems to show the effects of the late vertical mixing and thus has a tendency to overestimate the concentrations. The model also estimates deposition over the continent (Figure 9) similar to the estimations made by the FALL3D model ($\sim100\,g\,m^{-2}$) [*Collini et al.*, 2013]. From 4 to 14 June, HYSPLIT estimates the total deposition over Trelew to be $\sim70\,g\,m^{-2}$. During the same period, a minimum of $38\,g\,m^{-2}$ was measured at Trelew (Table 4), but considering the low efficiency of the CP collector (see section 3.1), this figure can be reestimated to be $110\,g\,m^{-2}$.

The agreement between data from the monitoring station and the models allows for the use of HYSPLIT outputs to estimate dissolved Fe inputs into the ocean. The model estimates ash deposition over an oceanic area of $\sim20\times10^6\,km^2$, which represents $\sim9.0\times10^{-2}\,km^3$ dense rock equivalent. About half of the oceanic area impacted by ash ($\sim11\times10^6\,km^2$) corresponds to HNLC oceanic regions. The model shows that approximately $9\times10^6\,km^2$ (dark green area in Figure 9) received ash deposition of >1 to $10\,g\,m^{-2}$, which was predominately composed of fine particles ($<11\,\mu m$).

The mean surface dissolved Fe in the South Atlantic and the Southern Ocean is $\sim0.29\,nmol/L$ [*Klunder et al.*, 2011; *Tagliabue et al.*, 2012; *Browning et al.*, 2014; *Rijkenberg et al.*, 2014]. Figure 10 shows the spatial variation
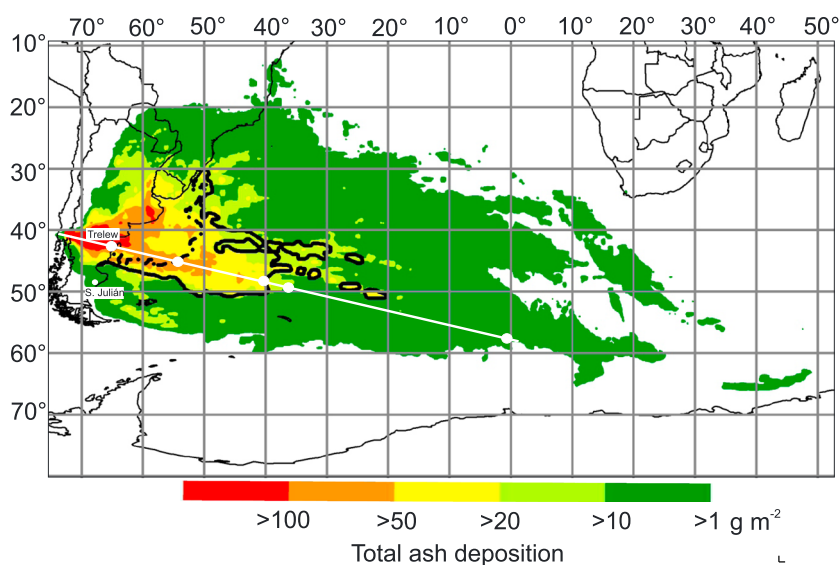
Figure 9. Total volcanic ash deposition modeled by HYSPLIT for the Puyehue eruption between 4 and 20 June 2011. Dashed black line and solid black line represent ash deposition with 50% and 75% of particles having grain size <11 μm, respectively. The white line connects the Puyehue volcano center to the city of Trelew and is projected to the open ocean. The white dots over the line represent the limits of main changes in ash deposition and particles grain size (see Figure 10).

of concentration of dissolved Fe supplied by volcanic ash plus the initial Fe concentration on the ocean surface. For these oceanic regions, a mixed layer depth of 100 m for wintertime can be assumed [*de Boyer Montégut et al.*, 2004], and thus, during the eruption, dry and wet depositions of ash near the coast (Trelew) could raise the initial oceanic dissolved Fe concentration by about 0.023 to 0.23 nmol/L. For distances >3000 km from the volcanic center, dry ash deposition could increase the oceanic dissolved Fe concentration by a range of 0.003 to 0.03 nmol/L and the wet deposition by a range of 0.015 to 0.13 nmol/L. Ash processed by acid volcanic plume could increase dissolved Fe concentration on the ocean surface 30 to 150 times more than wet and dry depositions [*Chen and Grassian*, 2013; *Cwiertny et al.*, 2008; *Solmon et al.*, 2009].

To initiate a phytoplankton bloom in iron-limited waters such as the Southern Ocean, the concentration of dissolved Fe throughout the mixed layer must reach a sustained threshold value of 0.5 nmol/L for at least 3 days [*Boyd and Ellwood*, 2010]. For a distance of up to 2000 km from the coast during austral winter, data indicate that only the upper bound of the added dissolved Fe concentration through wet deposition is slightly over this threshold (Figure 10). As observed, in the case of ash processed by acid volcanic plumes, the dissolved Fe is well above the 0.5 nmol/L threshold.

There are no reports about the existence of phytoplankton blooms in the Southern Ocean linked to the Puyehue eruption. One probable explanation is
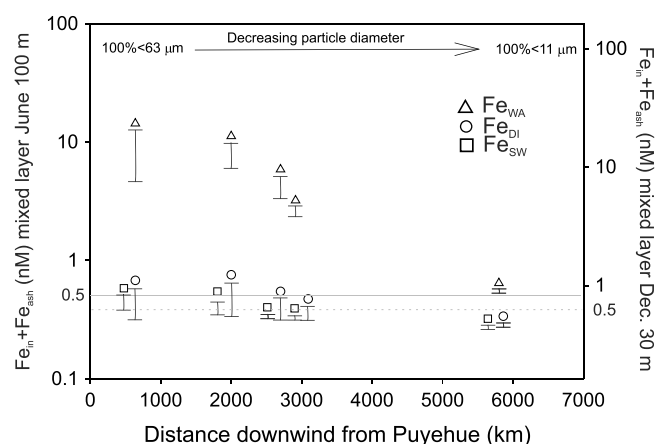

Figure 10. The *x* axis represents the white line and distances (white dots) from Figure 9 and shows the spatial variation of total dissolved Fe concentrations (mean Fe dissolved in the ocean or initial + Fe supplied by volcanic ash) simulating dry (Fe_{SW}) and wet (Fe_{DI} and Fe_{WA}) deposition over the South Atlantic/Southern Ocean. Concentrations show the range indicated by the minimum and the maximum release of Fe based on data from samples P6 to P8 (Table 2). The threshold seawater concentrations for initiate a phytoplankton bloom are indicated as solid (winter) and dashed (summer) lines.

that the low solar irradiation during winter discourages phytoplankton blooms. As volcanic eruptions occur randomly, a second scenario, which assumes that the Pueyehue eruption took place during austral summer (mixed layer at 30 m) [*de Boyer Montégut et al.*, 2004], indicates that for important oceanic areas, the input of dissolved Fe through dry and wet ash depositions would reach values over the 0.5 nmol/L threshold (Figure 10).

Based on data from the monitoring station, we deduce that a 14 day eruption, like the Pueyehue volcano, can contribute ~15 to 160 more times (dry and wet depositions, respectively) dissolved Fe to the Argentinean shelf than the contribution of typical Patagonian dust during the same period.

5. Conclusions

Three of the largest volcanic eruptions that occurred in the last 22 years in the southern Andes have contributed different amounts and compositions of ash to the South Atlantic sector of the Southern Ocean. When andesitic-type materials (Hudson volcano) are simulated in contact with acidic waters such as those predominating in clouds, an enhanced dissolution of Fe-bearing salts is observed, which results in higher Fe liberation to the aqueous phase and faster release rates. This behavior can be partially explained by the presence of soluble salts with a relative abundance of Fe^{2+}. On the other hand, the rhyolitic-type eruption (Chaitén volcano) contributed lower amount of ashes to the ocean surface. Rhyolitic ashes seem less affected by acid leaching during plume process. When processed by cloud water, they could potentially release less Fe and have slower rate dissolution of this metal.

The chemical composition of ashes also determines the amount and velocity of Fe release in contact with seawater. In contrast to our observations after treatment with deionized water, the solubility of Fe in contact with seawater is higher in rhyolitic-type ashes and lower in andesitic ashes.

Chemical reactions, such as acid processing on volcanic ash surfaces, are common phenomena during explosive volcanic eruptions and represent an important soluble Fe transfer mechanism to the ocean surface. The simulation of the development of acidic conditions during the plume process promotes Fe increased solubility of ash particles. However, the separation of the phases that contribute Fe under these conditions is challenging; we infer that these could be mainly associated with reducible phases, present as a coating of finer ash crystalline particles. Silicic-rich ashes under acidic conditions release Fe in higher amounts and at a slower rate, while in samples containing mostly glass shards, the amount of Fe released was lower and faster.

For the first time in Patagonia, the evolution of fluxes and concentrations of a volcanic plume has been observed. The Puyehue eruption event was intercepted in its trajectory to the Southern Ocean through a monitoring station placed >500 km from the volcanic center. These materials have shown to have intermediate values between andesitic and rhyolitic compositions. Thus, the magnitude of the eruption and the intermediate chemical composition of the ashes make the Puyehue event a representative case study of the potential amount of soluble Fe supplied to the ocean surface after a southern Andean volcanic event. In terms of the amount of ashes supplied to the ocean, the Puyehue contribution was 10 times lower than the Hudson and 10 times larger than the Chaitén event. Taking into account the initial dissolved Fe on the ocean surface, a Puyehue-type eruption could contribute soluble Fe (through dry or wet deposition) to nearly or just reach the limit required for phytoplankton growth in the Southern Ocean. On the other hand, the input of soluble Fe after the acidic process of ash particles can raise the amount of dissolved Fe on the surface of the ocean several times, well above the threshold required to initiate phytoplankton blooms. Rhyolitic eruptions contribute less dissolved Fe to the ocean surface, suggesting that this particular event would not trigger a bloom even if it took place during summer. Nevertheless, a similar analysis done with the Hudson eruption indicates that this event could contribute several times more soluble iron to the ocean surface than the amount contributed by the eruptions of the Pueyhue and Chaitén volcanoes. These findings agree with *Langmann* [2014], who indicates that the Hudson eruption was never taken into account as an explanation for the decrease in atmospheric CO_2 concentration by 1–2 ppm after 1991, an event which has normally been attributed to the Pinatubo eruption.

Up to now, there have not been any reports indicating a biological response by the surface of the South Atlantic/Southern Ocean after ash inputs from the three eruptions considered in this contribution. A main

reason for this could be associated with the lower intensity of the eruptions of the more silicic events (e.g., Puyehue and Chaitén). Another reason could be linked to the fact that the eruptions occurred during austral winter, when sunlight is an extra factor limiting phytoplankton bloom. Westerlies winds intensify during springtime-summertime, and intense ash remobilization from the Patagonian surface is expected for several months after the main eruptions, raising the typical dust flux background of the region. However, our data indicate that the volcanic ash mixed with Patagonian soils results in lower Fe solubility, and data from the monitoring station show that even if background dust fluxes increased after the Puyehue eruption, they were at much lower values than those observed during the volcanic eruption.

The three types of materials studied in this paper have increased our understanding of the solubility and mineralogical control of Fe in volcanic ash and could contribute to improved model estimations. Late Quaternary eruptions from volcanoes in the southern Andes have deposited extensive volumes of andesitic to rhyolitic ash into the Atlantic/Southern Ocean. Both the intensity and composition of such volcanic events have been recorded in terrestrial and oceanic paleo-archives. Our study can improve interpretations of historical volcanic eruptions and their climate impact, considering their potential fertilization effect on key oceanic areas such as the Southern Ocean.

References

Achterberg, E. P., et al. (2013), Natural iron fertilization by the Eyjafjallajokull volcanic eruption, *Geophys. Res. Lett.*, *40*, 921–926, doi:10.1002/grl.50221.

Alfano, F., C. Bonadonna, A. C. M. Volentik, C. B. Connor, S. F. L. Watt, D. M. Pyle, and L. J. Connor (2011), Tephra stratigraphy and eruptive volume of the May, 2008, Chaitén eruption, Chile, *Bull. Volcanol.*, *73*(5), 613–630.

Armienta, M. A. Á., S. De Cruz-reyna, O. Morton, O. Cruz, and N. Ceniceros (2002), Chemical variations of tephra-fall deposit leachates for three eruptions from Popocatepelt volcano, *J. Volcanol. Geotherm. Res.*, *113*(1–2), 61–80.

Ayris, P., and P. Delmelle (2012), Volcanic and atmospheric controls on ash iron solubility: A review, *Phys. Chem. Earth, Parts A/B/C*, *45–46*, 103–112.

Baker, A. R., and P. L. Croot (2010), Atmospheric and marine controls on aerosol iron solubility in seawater, *Mar. Chem.*, *120*(1–4), 4–13, doi:10.1016/j.marchem.2008.09.003.

Baker, A. R., C. Adams, T. G. Bell, T. D. Jickells, and L. Ganzeveld (2013), Estimation of atmospheric nutrient inputs to the Atlantic Ocean from 50°N to 50°S based on large-scale field sampling: Iron and other dust-associated elements, *Global Biogeochem. Cycles*, *27*, 755–767, doi:10.1002/gbc.20062.

Bermudez, A., and D. Delpino (2011), La actividad el volcán Puyehue y su impacto sobre el territorio de la República Argentina, Primer Informe, Neuquén, 14 de Junio de 2011.

Bia, G., L. Borgnino, D. Gaiero, and M. G. García (2015), Arsenic-bearing phases in South Andean volcanic ashes: Implications for As mobility in aquatic environments, *Chem. Geol.*, *393–394*, 26–35.

Botto, I. L., M. E. Canafoglia, D. Gazzoli, and M. J. González (2013), Spectroscopic and microscopic characterization of volcanic ash from Puyehue-(Chile) eruption: Preliminary approach for the application in the arsenic removal, *J. Spectrosc.*, *2013*, 254517.

Boyd, P. W., and M. J. Ellwood (2010), The biogeochemical cycle of iron in the ocean, *Nat. Geosci.*, *3*(10), 675–682.

Browning, T. J., H. A. Bouman, G. M. Henderson, T. A. Mather, D. M. Pyle, C. Schlosser, E. M. S. Woodward, and C. M. Moore (2014), Strong responses of Southern Ocean phytoplankton communities to volcanic ash, *Geophys. Res. Lett.*, *41*, 2851–2857, doi:10.1002/2014GL059364.

Castro, J. M., and D. B. Dingwell (2009), Rapid ascent of rhyolitic magma at Chaitén volcano, Chile, *Nature*, *461*(7265), 780–783.

Cather, S. M., N. W. Dunbar, F. W. McDowell, W. C. McIntosh, and P. A. Scholle (2009), Climate forcing by iron fertilization from repeated ignimbrite eruptions: The icehouse–silicic large igneous province (SLIP) hypothesis, *Geosphere*, *5*, 315–324.

Chate, D. M., and P. C. S. Devara (2009), Acidity of raindrop by uptake of gases and aerosol pollutants, *Atmos. Environ.*, *43*, 1571–1577.

Chen, H., and V. H. Grassian (2013), Iron dissolution of dust source materials during simulated acidic processing: The effect of sulfuric, acetic, and oxalic acids, *Environ. Sci. Technol.*, *47*(18), 10,312–10,321.

Collini, E., M. S. Osores, A. Folch, J. G. Viramonte, G. Villarosa, and G. Salmuni (2013), Volcanic ash forecast during the June 2011 Cordón Caulle eruption, *Nat. Hazards*, *66*, 389–412.

Croot, P. L., and M. I. Heller (2012), The importance of kinetics and redox in the biogeochemical cycling of iron in the surface ocean, *Front. Microbiol.*, *3*, 219.

Croot, P. L., and M. Johansson (2000), Determination of iron speciation by cathodic stripping voltammetry in seawater using the competing ligand 2-(2-Thiazolylazo)-p-cresol (TAC), *Electroanalysis*, *12*, 565–576.

Cwiertny, D. M., J. Baltrusaitis, G. J. Hunter, A. Laskin, M. M. Scherer, and V. H. Grassian (2008), Characterization and acid-mobilization study of iron-containing mineral dust source materials, *J. Geophys. Res.*, *113*, D05202, doi:10.1029/2007JD009332.

De Boyer Montégut, C., G. Madec, A. S. Fischer, A. Lazar, and D. ludicone (2004), Mixed layer depth over the global ocean: An examination of profile data and a profile-based climatology, *J. Geophys. Res.*, *109*, C12003, doi:10.1029/2004JC002378.

Delmelle, P., M. Lambert, Y. Dufrene, P. Gerin, and N. Oskarsson (2007), Gas/aerosol-ash interaction in volcanic plumes: New insights from surface analyses of fine ash particles, *Earth Planet. Sci. Lett.*, *259*(1–2), 159–170.

Draxler, R. R., and G. D. Hess (1998), An overview of the HYSPLIT_4 modelling system for trajectories, *Aust. Meteorol. Mag.*, *47*(4), 295–308.

Duggen, S., P. Croot, U. Schacht, and L. Hoffmann (2007), Subduction zone volcanic ash can fertilize the surface ocean and stimulate phytoplankton growth: Evidence from biogeochemical experiments and satellite data, *Geophys. Res. Lett.*, *34*, L01612, doi:10.1029/2006GL027522.

Durant, A. J., G. Villarosa, W. I. Rose, P. Delmelle, A. J. Prata, and J. G. Viramonte (2012), Long-range volcanic ash transport and fallout during the 2008 eruption of Chaitén volcano, Chile, *Phys. Chem. Earth, Parts A/B/C*, *45–46*, 50–64.

Falkowski, P. G., R. T. Barber, and V. Smetacek (1998), Biogeochemical controls and feedbacks on ocean primary production, *Science*, *281*(5374), 200–206.

Folch, A., O. Jorba, and J. Viramonte (2008), Volcanic ash forecast—Application to the May 2008 Chaiten eruption, *Earth*, *8*(4), 927–940.

Frogner, P., S. R. Gíslason, and N. Óskarsson (2001), Fertilizing potential of volcanic ash on ocean surface water, *Geology*, *29*(6), 487–490.

Fryrear, D. W. (1986), A field dust sampler, *J. Soil Water Conserv.*, *41*(2), 117–120.

Gaiero, D. M., J.-L. Probst, P. J. Depetris, S. M. Bidart, and L. Leleyter (2003), Iron and other transition metals in Patagonian riverborne and windborne materials: Geochemical control and transport to the southern South Atlantic Ocean, *Geochim. Cosmochim. Acta*, *67*(19), 3603–3623.

Gaiero, D. M., L. Simonella, S. Gassó, S. Gili, A. F. Stein, P. Sosa, R. Becchio, J. Arce, and H. Marelli (2013), Ground/satellite observations and atmospheric modeling of dust storms originating in the high Puna-Altiplano deserts (South America): Implications for the interpretation of paleo-climatic archives, *J. Geophys. Res. Atmos.*, *118*, 3817–3831, doi:10.1002/jgrd.50036.

Gangale, G., A. J. Prata, and L. Clarisse (2010), The infrared spectral signature of volcanic ash 715 determined from high-spectral resolution satellite measurements, *Remote Sens. Environ.*, *114*(2), 414–425.

Gassó, S., and A. F. Stein (2007), Does dust from Patagonia reach the sub-Antarctic Atlantic Ocean?, *Geophys. Res. Lett.*, *34*, L01801, doi:10.1029/2006GL027693.

Gassó, S., A. Stein, F. Marino, E. Castellano, R. Udisti, and J. Ceratto (2010), A combined observational and modeling approach to study modern dust transport from the Patagonia desert to East Antarctica, *Atmos. Chem. Phys.*, *10*(17), 8287–8303.

Gislason, S. R., et al. (2011), Characterization of Eyjafjallajökull volcanic ash particles and a protocol for rapid risk assessment, *Proc. Natl. Acad. Sci. U.S.A.*, *108*(18), 7307–7312.

Global Volcanism Network Bulletin (1991), *Smithsonian Institution*, vol. 16, pp. 2–4, AGU, Washington, D. C.

Goossens, D., and B. J. Buck (2012), Can BSNE (Big Spring Number Eight) samplers be used to measure PM10, respirable dust, PM2.5 and PM1.0?, *Aeolian Res.*, *5*, 43–49.

Goossens, D., and J. L. Rajot (2008), Techniques to measure the dry aeolian deposition of dust in arid and semi-arid landscapes: A comparative study in Sahelian West Africa, *Earth Surf. Processes Landforms*, *33*, 178–195.

Hamilton, J. P., and C. G. Pantano (2000), Dissolution of albite glass and crystal, *Geochim. Cosmochim. Acta*, *64*, 2603–2615.

Hamme, R. C., et al. (2010), Volcanic ash fuels anomalous plankton bloom in subarctic northeast Pacific, *Geophys. Res. Lett.*, *37*, L19604, doi:10.1029/2010GL044629.

He, K., Q. Zhao, Y. Ma, F. Duan, F. Yang, Z. Shi, and G. Chen (2012), Spatial and seasonal variability of PM2.5 acidity at two Chinese megacities: Insights into the formation of secondary inorganic aerosols, *Atmos. Chem. Phys.*, *12*, 1377–1395.

Heffter, J. L., and B. J. B. Stunder (1993), Volcanic Ash Forecast Transport and Dispersion (VAFTAD) model, *Weather Forecasting*, *8*, 533–541.

Iglesias, V., C. Whitlock, M. M. Bianchi, G. Villarosa, and V. Outes (2012), Holocene climate variability and environmental history at the Patagonian forest/steppe ecotone: Lago Mosquito (42° 29′37.89″S, 71° 24′14.57″W) and Laguna del Cóndor (42° 20′47.22″S, 71° 17′07.62″W), *Holocene*, *22*(11), 1297–1307.

Jickells, T. D., and L. J. Spokes (2001), Atmospheric iron inputs to the oceans, in *Biogeochemistry of Iron in Seawater*, IUPAC Book Ser. Anal. Phys. Chem. Environ. Syst., pp. 85–122, John Wiley Ltd., Chichester, U. K.

Jickells, T. D., et al. (2005), Global iron connections between desert dust, ocean biogeochemistry, and climate, *Science*, *308*(5718), 67–71.

Johnson, M. S., N. Meskhidze, F. Solmon, S. Gassó, P. Y. Chuang, D. M. Gaiero, R. M. Yantosca, S. Wu, Y. Wang, and C. Carouge (2010), Modeling dust and soluble iron deposition to the South Atlantic Ocean, *J. Geophys. Res.*, *115*, D15202, doi:10.1029/2009JD013311.

Jones, M. T., and S. R. Gislason (2008), Rapid releases of metal salts and nutrients following the deposition of volcanic ash into aqueous environments, *Geochim. Cosmochim. Acta*, *72*(15), 3661–3680.

Journet, E., K. V. Desboeufs, S. Caquineau, and J.-L. Colin (2008), Mineralogy as a critical factor of dust iron solubility, *Geophys. Res. Lett.*, *35*, L07805, doi:10.1029/2007GL031589.

Kalnay, E., et al. (1996), The NCEP/NCAR 40-year reanalysis project, *Bull. Am. Meteorol. Soc.*, *77*(3), 437–471.

Kanamitsu, M. (1989), Description of the NMC global data assimilation and forecast system, *Weather Forecasting*, *4*, 335–342.

Klunder, M. B., P. Laan, R. Middag, H. de Baar, and J. C. van Ooijen (2011), Dissolved iron in the Southern Ocean (Atlantic sector), *Deep Sea Res., Part II*, *58*(25–16), 2678–2694.

Kratzmann, D. J., S. Carey, R. Scasso, and J. A. Naranjo (2009), Compositional variations and magma mixing in the 1991 eruptions of Hudson volcano, Chile, *Bull. Volcanol.*, *71*(4), 419–439.

Kunz-Pirrung, M., R. Gersonde, and D. A. Hodell (2002), Mid-Brunhes century-scale diatom sea surface temperature and sea ice records from the Atlantic sector of the Southern Ocean (ODP Leg 177, sites 1093, 1094 and core PS2089-2), *Palaeogeogr. Palaeoclimatol. Palaeoecol.*, *182*(3–4), 305–328.

Langmann, B. (2014), On the role of climate forcing by volcanic sulphate and volcanic ash, *Adv. Meteorol.*, *2014*, 340123.

Langmann, B., K. Zaksek, M. Hort, and S. Duggen (2010), Volcanic ash as fertiliser for the surface ocean, *Atmos. Chem. Phys.*, *10*, 3891–3899.

Lara, L. E. (2009), The 2008 eruption of the Chaiten Volcano, Chile: A preliminary report, *Andean Geol.*, *36*(1), 125–129.

Li, F., P. Ginoux, and V. Ramaswamy (2008), Distribution, transport, and deposition of mineral dust in the Southern Ocean and Antarctica: Contribution of major sources, *J. Geophys. Res.*, *113*, D10207, doi:10.1029/2007JD009190.

Mahowald, N. M., D. R. Muhs, S. Levis, P. J. Rasch, M. Yoshioka, C. S. Zender, and C. Luo (2006), Change in atmospheric mineral aerosols in response to climate: Last glacial period, preindustrial, modern, and doubled carbon dioxide climates, *J. Geophys. Res.*, *111*, D10202, doi:10.1029/2005JD006653.

Martin, J. H., S. E. Fitzwater, and R. M. Gordon (1990), Iron deficiency limits phytoplankton growth in Antarctic waters, *Global Biogeochem. Cycles*, *4*(1), 5–12, doi:10.1029/GB004i001p00005.

Martínez-Garcia, A., A. Rosell-Melé, S. L. Jaccard, W. Geibert, D. M. Sigman, and G. H. Haug (2011), Southern Ocean dust-climate coupling over the past four million years, *Nature*, *476*(7360), 312–315.

Mastin, L. G., et al. (2009a), A multidisciplinary effort to assign realistic source parameters to models of volcanic ash-cloud transport and dispersion during eruptions, *J. Volcanol. Geotherm. Res.*, *186*(1–2), 10–21.

Mastin, L. G., M. Guffanti, J. E. Ewert, and J. Spiegel (2009b), Preliminary spreadsheet of eruption source parameters for volcanoes of the world, *U.S. Geol. Surv. Open File Rep., 2009-1133*, version 1.2.

Mélançon, J., et al. (2014), Early response of the northeast subarctic Pacific plankton assemblage to volcanic ash fertilization, *Limnol. Oceanogr.*, *59*(1), 55–67.

Meskhidze, N., W. L. Chameides, A. Nenes, and G. Chen (2003), Iron mobilization in mineral dust: Can anthropogenic SO_2 emissions affect ocean productivity?, *Geophys. Res. Lett.*, *30*(21), 2085, doi:10.1029/2003GL018035.

Morel, F. M. M., and N. M. Price (2003), The biogeochemical cycles of trace metals in the oceans, *Science*, *300*(5621), 944–947.

Murad, E. (2010), Mössbauer spectroscopy of clays, soils and their mineral constituents, *Clay Miner.*, *45*(4), 413–430.

Naranjo, J. A., and C. R. Stern (1998), Holocene explosive activity of Hudson volcano, southern Andes, *Bull. Volcanol.*, *59*(4), 291–306.

Naranjo, J. A., and C. R. Stern (2004), Holocene tephrochronology of the southernmost part (42 degrees 30'–45 degrees S) of the Andean Southern Volcanic Zone, *Rev. Geol. Chile*, *31*(2), 225–240.

Nenes, A., M. D. Krom, N. Mihalopoulos, P. Van Cappellen, Z. Shi, A. Bougiatioti, P. Zarmpas, and B. Herut (2011), Atmospheric acidification of mineral aerosols: A source of bioavailable phosphorus for the oceans, *Atmos. Chem. Phys. Discuss.*, *11*(2), 6163–6185.

Olgun, N., S. Duggen, P. L. Croot, P. Delmelle, H. Dietze, U. Schacht, N. Óskarsson, C. Siebe, A. Auer, and D. Garbe-Schönberg (2011), Surface ocean iron fertilization: The role of airborne volcanic ash from subduction zone and hot spot volcanoes and related iron fluxes into the Pacific Ocean, *Global Biogeochem. Cycles*, *25*, GB4001, doi:10.1029/2009GB003761.

Olgun, N., S. Duggen, D. Andronico, S. Kutterolf, P. L. Croot, S. Giammanco, P. Censi, and L. Randazzo (2013), Possible impacts of volcanic ash emissions of Mount Etna on the primary productivity in the oligotrophic Mediterranean Sea: Results from nutrient-release experiments in seawater, *Mar. Chem.*, *152*, 32–42.

Olsson, J., S. L. S. Stipp, K. N. Dalby, and S. R. Gislason (2013), Rapid release of metal salts and nutrients from the 2011 Grímsvötn, Iceland volcanic ash, *Geochim. Cosmochim. Acta*, *123*, 134–149.

Olsson, J., S. L. S. Stipp, E. Makovicky, and S. R. Gislason (2014), Metal scavenging by calcium carbonate at the Eyjafjallajökull volcano: A carbon capture and storage analogue, *Chem. Geol.*, *384*, 135–148.

Orange, D., J. Y. Gac, J. L. Probst, and D. Tanre (1990), Mesure du dépôt au sol des aérosol désertiques. Une méthode simple de prélèvement: Le capteur pyramidal, *C. R. Acad. Sci. Paris*, *311*(2), 167–172.

Raiswell, R., and D. E. Canfield (2012), The iron biogeochemical cycle past and present, *Geochem. Perspect.*, *1*, 1–220.

Rijkenberg, M. J. A., R. Middag, P. Laan, L. J. A. Gerringa, H. M. van Aken, V. Schoemann, J. T. M. de Jong, and H. J. W. de Baar (2014), The distribution of dissolved iron in the west Atlantic Ocean, *PLoS One*, *9*(6), e101323.

Rogers, N., and C. Hawkesworth (2000), Composition of magmas, in *Encyclopedia of Volcanoes*, edited by H. Sigurdsson et al., pp. 115–131, Academic Press, London.

Ruggieri, F., J. Saavedra, J. L. Fernandez-Turiel, D. Gimeno, and M. Garcia-Valles (2010), Environmental geochemistry of ancient volcanic ashes, *J. Hazard. Mater.*, *183*(1–3), 353–365.

Ruggieri, F., J. L. Fernandez-Turiel, J. Saavedra, D. Gimeno, E. Polanco, A. Amigo, G. Galindo, and A. Caselli (2012), Contribution of volcanic ashes to the regional geochemical balance: The 2008 eruption of Chaitén volcano, Southern Chile, *Sci. Total Environ.*, *425*, 75–88.

Sarmiento, J. L. (1993), Atmospheric CO2 stalled, *Nature*, *365*, 697–698.

Sarmiento, J. L., R. D. Slater, M. J. R. Fasham, H. W. Ducklow, J. R. Toggweiler, and G. T. Evans (1993), A seasonal 3-dimensional ecosystem model of nitrogen cycling in the North-Atlantic Euphotic Zone, *Global Biogeochem. Cycles*, *7*(2), 417–450, doi:10.1029/93GB00375.

Scasso, R. A., H. Corbella, and P. Tiberi (1994), Sedimentological analysis of the tephra from the 12–15 August 1991 eruption of Hudson volcano, *Bull. Volcanol.*, *56*(2), 121–132.

Schroth, A. W., J. Crusius, E. R. Sholkovitz, and B. C. Bostick (2009), Iron solubility driven by speciation in dust sources to the ocean, *Nat. Geosci.*, *2*, 337–340.

Seinfeld, J. H., and S. N. Pandis (2006), *Atmospheric Chemistry and Physics: From Air Pollution to Climate Change*, John Wiley, New York.

Shi, Z., S. Bonneville, M. D. Krom, K. S. Carslaw, T. D. Jickells, A. R. Baker, and L. G. Benning (2011), Iron dissolution kinetics of mineral dust at low pH during simulated atmospheric processing, *Atmos. Chem. Phys.*, *11*(3), 995–1007.

Shi, Z., M. Krom, T. Jickells, and S. Bonneville (2012), Impacts on iron solubility in the mineral dust by processes in the source region and the atmosphere: A review, *Aeolian Res.*, *5*, 21–42.

Simonella, L. E., D. M. Gaiero, and M. E. Palomeque (2014), Validation of a continuous flow method for the determination of soluble iron in atmospheric dust and volcanic ash, *Talanta*, *128*, 248–253.

Singer, B. S., B. R. Jicha, M. A. Harper, J. A. Naranjo, L. E. Lara, and H. Moreno-Roa (2008), Eruptive history, geochronology, and magmatic evolution of the Puyehue-Cordon Caulle volcanic complex, Chile, *Geol. Soc. Am. Bull.*, *120*(5), 599–618.

Skamarock, W. C., J. B. Klemp, J. Dudhia, D. Gill, D. M. Barjer, M. G. Duda, X. Y. Huang, W. Wang, and J. G. Powers (2008), A description of the advanced research WRF version 3, NCAR Tech Note NCAR/TN-475+STR 125.

Skonieczny, C., et al. (2011), The 7–13 March 2006 major Saharan outbreak: Multiproxy characterization of mineral dust deposited on the West African margin, *J. Geophys. Res.*, *116*, D18210, doi:10.1029/2011JD016173.

Smellie, J. L. (1999), The upper Cenozoic tephra record in the south polar region: A review, *Global Planet. Change*, *21*(1–3), 51–70.

Solmon, F., P. Y. Chuang, N. Meskhidze, and Y. Chen (2009), Acidic processing of mineral dust iron by anthropogenic compounds over the north Pacific Ocean, *J. Geophys. Res.*, *114*, D02305, doi:10.1029/2008JD010417.

Spokes, L. J., and T. D. Jickells (1996), Factors controlling the solubility of aerosol trace metals in the atmosphere and on mixing into seawater, *Aquat. Geochem.*, *1*, 355–374.

Stunder, B. J. B., J. L. Heffter, and R. R. Draxler (2007), Airborne volcanic ash forecast area reliability, *Weather Forecasting*, *22*, 1132–1139.

Sunda, W. G., and S. A. Huntsman (1995), Iron uptake and growth limitation in oceanic and coastal phytoplankton, *Mar. Chem.*, *50*(1–4), 189–206.

Tagliabue, A., T. Mtshali, O. Aumont, A. R. Bowie, M. B. Klunder, A. N. Roychoudhury, and S. Swart (2012), A global compilation of dissolved iron measurements: Focus on distributions and processes in the Southern Ocean, *Biogeosciences*, *9*(6), 2333–2349.

Thorsteinsson, T., T. Jóhannsson, A. Stohl, and N. I. Kristiansen (2012), High levels of particulate matter in Iceland due to direct ash emissions by the Eyjafjallajökull eruption and resuspension of deposited ash, *J. Geophys. Res.*, *117*, B00C05, doi:10.1029/2011JB008756.

Toscano, G., C. Caristi, and G. Cimino (2008), Sorption of heavy metal from aqueous solution by volcanic ash, *C. R. Chim.*, *11*(6–7), 765–771.

Vandenberghe, R. E. (1991), *Mössbauer Spectroscopy and Applications in Geology*, International Training Center for Post- Graduate Soil Scientists, Ghent, Belgium.

Watson, A. J. (1997), Volcanic Fe, CO2, ocean productivity and climate, *Nature*, *385*, 587–588.

Watt, S. F. L., D. M. Pyle, T. A. Mather, R. S. Martin, and N. E. Matthews (2009), Fallout and distribution of volcanic ash over Argentina following the May 2008 explosive eruption of Chaitén, Chile, *J. Geophys. Res.*, *114*, B04207, doi:10.1029/2008JB006219.

Witham, C. S., C. Oppenheimer, and C. J. Horwell (2005), Volcanic ash-leachates: A review and recommendations for sampling methods, *J. Volcanol. Geotherm. Res.*, *141*(3–4), 299–326.

Wolff-Boenisch, D., S. R. Gislason, and E. H. Oelkers (2006), The effect of crystallinity on dissolution rates and CO2 consumption capacity of silicates, *Geochim. Cosmochim. Acta*, *70*(4), 858–870.